NAVAL POSTGRADUATE SCHOOL

MONTEREY, CALIFORNIA

THESIS

UPPER-LEVEL BLACK SEA LOW: DIAGNOSING CYCLOGENESIS LEE OF THE MIDDLE TAURUS MOUNTAINS

by

Jason J. Senter

March 2020

Thesis Advisor: Wendell A. Nuss
Second Reader: Scott Powell

THIS PAGE INTENTIONALLY LEFT BLANK

REPORT DOCUMENTATION PAGE			*Form Approved OMB No. 0704-0188*

1. AGENCY USE ONLY *(Leave blank)*	**2. REPORT DATE** March 2020	**3. REPORT TYPE AND DATES COVERED** Master's thesis

4. TITLE AND SUBTITLE
UPPER-LEVEL BLACK SEA LOW: DIAGNOSING CYCLOGENESIS LEE OF THE MIDDLE TAURUS MOUNTAINS

5. FUNDING NUMBERS

6. AUTHOR(S) Jason J. Senter

7. PERFORMING ORGANIZATION NAME(S) AND ADDRESS(ES)
Naval Postgraduate School
Monterey, CA 93943-5000

8. PERFORMING ORGANIZATION REPORT NUMBER

9. SPONSORING / MONITORING AGENCY NAME(S) AND ADDRESS(ES)
N/A

10. SPONSORING / MONITORING AGENCY REPORT NUMBER

11. SUPPLEMENTARY NOTES The views expressed in this thesis are those of the author and do not reflect the official policy or position of the Department of Defense or the U.S. Government.

12a. DISTRIBUTION / AVAILABILITY STATEMENT
Approved for public release. Distribution is unlimited.

12b. DISTRIBUTION CODE
A

13. ABSTRACT (maximum 200 words)

An upper-level trough that transited the Black Sea to the lee side of the Middle Taurus Mountains in Southern Turkey is analyzed over the course of three days, from 1200 UTC 17 February to 0000 UTC 20 February 2015. Analysis of this storm, using CFSR re-analysis output as a means to identify a cut-off, upper-level low, with associated downstream sensible weather in the Tigris-Euphrates River Valleys, is a crucial first step in locating a quasi-stationary system. This type of an anomalous event proves challenging for forecasters in predicting timing and impacts in the region. Identifying and describing the dynamical elements of this system as they unfolded lee of the Middle Taurus Mountains utilizing a fine scale WRF simulation revealed a unique relationship of the topography and the upper-level trough. This ability to show a connection of orographic, low-level forcing to upper-level disturbances is the first step in accurately predicting cloud coverage, precipitation, and wind speeds, which are all critical thresholds in forecasting for an area of operation (AO).

14. SUBJECT TERMS lee cyclogenesis, synoptic, mesoscale, potential vorticity	**15. NUMBER OF PAGES** 63
	16. PRICE CODE

17. SECURITY CLASSIFICATION OF REPORT	**18. SECURITY CLASSIFICATION OF THIS PAGE**	**19. SECURITY CLASSIFICATION OF ABSTRACT**	**20. LIMITATION OF ABSTRACT**
Unclassified	Unclassified	Unclassified	UU

NSN 7540-01-280-5500

Standard Form 298 (Rev. 2-89)
Prescribed by ANSI Std. 239-18

THIS PAGE INTENTIONALLY LEFT BLANK

Approved for public release. Distribution is unlimited.

UPPER-LEVEL BLACK SEA LOW: DIAGNOSING CYCLOGENESIS LEE OF THE MIDDLE TAURUS MOUNTAINS

Jason J. Senter
Captain, United States Air Force
BS, University of Missouri - Columbia, 2013

Submitted in partial fulfillment of the
requirements for the degree of

MASTER OF SCIENCE IN METEOROLOGY

from the

NAVAL POSTGRADUATE SCHOOL
March 2020

Approved by: Wendell A. Nuss
Advisor

Scott Powell
Second Reader

Wendell A. Nuss
Chair, Department of Meteorology

THIS PAGE INTENTIONALLY LEFT BLANK

ABSTRACT

An upper-level trough that transited the Black Sea to the lee side of the Middle Taurus Mountains in Southern Turkey is analyzed over the course of three days, from 1200 UTC 17 February to 0000 UTC 20 February 2015. Analysis of this storm, using CFSR re-analysis output as a means to identify a cut-off, upper-level low, with associated downstream sensible weather in the Tigris-Euphrates River Valleys, is a crucial first step in locating a quasi-stationary system. This type of an anomalous event proves challenging for forecasters in predicting timing and impacts in the region. Identifying and describing the dynamical elements of this system as they unfolded lee of the Middle Taurus Mountains utilizing a fine scale WRF simulation revealed a unique relationship of the topography and the upper-level trough. This ability to show a connection of orographic, low-level forcing to upper-level disturbances is the first step in accurately predicting cloud coverage, precipitation, and wind speeds, which are all critical thresholds in forecasting for an area of operation (AO).

THIS PAGE INTENTIONALLY LEFT BLANK

TABLE OF CONTENTS

THIS PAGE INTENTIONALLY LEFT BLANK

LIST OF FIGURES

LIST OF TABLES

THIS PAGE INTENTIONALLY LEFT BLANK

LIST OF ACRONYMS AND ABBREVIATIONS

AMS	American Meteorological Society
CAA	cold air advection
CFS	climate forecast system
CFSR	climate forecast system reanalysis
GARP	(GEMPAK) Analysis and Rendering Program
GEMPAK	general meteorological package files
GHT	geopotential height (m)
GIBBS	Global International Satellite Cloud Project (ISCCP) B1 Browse System
ISCCP	International Satellite Cloud Project
METAR	meteorological aerodrome reports
MSLP	mean sea level pressure (hPa)
NCAR	National Center for Atmospheric Research
NCEI	National Centers for Environmental Information
NCEP	National Centers for Environmental Prediction
NMC	National Meteorological Center
NOAA	National Oceanographic and Atmospheric Administration
PVU	potential vorticity units ($10^{-6}s^{-1}\frac{K}{mb}$)
TROWAL	trough of warm air aloft
TRV-ERV	Tigris River Valley-Euphrates River Valley
UCAR	University Corporation for Atmospheric Research
UL-BSL	upper level-Black Sea low
WAA	warm air advection

THIS PAGE INTENTIONALLY LEFT BLANK

ACKNOWLEDGMENTS

I would first like to thank my wife for giving me the support and love necessary for the completion of this project. It is also pertinent to recognize my parents, and my brother, Thomas, as the driving forces behind my educational and professional careers by giving me their support and offering motivation through both my successes and failures along this journey. Thank you to my advisor, Dr. Wendel Nuss, and second reader, Dr. Scott Powell, as well as to the NPS meteorology staff and the NPS writing center for coaching and assisting me along the way. A special thanks to Dr. Frank Narducci and Dr. Jeffery Lee, for helping in the development of the numerical integration process. I would also like to thank the men and women with whom I served overseas who inspired me to tackle this topic of interest. The trust they bestowed on me and my team allowed us to dig even further into the roles and responsibilities as being both forecasters and, most importantly, effective team members.

THIS PAGE INTENTIONALLY LEFT BLANK

I. INTRODUCTION

A. BACKGROUND

Scientists around the world have studied, explained and quantified the regional impacts of orographic forcing on the development of cyclones. The primitive descriptions of extratropical cyclogenesis events described by Pettersen and Smebye (1971) characterizes the "Type B" cyclone as the development that commences with the invigoration of a region of warm air advection (WAA), or the absence of cold air advection (CAA), by an upper tropospheric region of positive vorticity advection. This pre-existing region of WAA lee of topography generates a low-level vorticity anomaly, which then interacts with the upper-level vorticity maxima to cause cyclogenesis. In the lee of topography, the scale of the orographic forcing has to be large enough in magnitude so that the retardation of CAA by the topography is sufficient to generate a low-level cyclone. The phases of cyclogenesis in the lee of topography, as described by Hoskins et al. (1985) and Tafferner (1990), follows the potential vorticity invertibility principle in which the low-level vortex associated with a surface thermal anomaly and/or a low-level potential vorticity anomaly grows over time as the upper levels interact. Furthermore, the downstream environment must be structured in such a way that maintains the low-level vortex for a sufficient amount of time prior to the amplification of a "phase-locked" vortex to occur. This "phased-lock" vortex refers to the baroclinic development of a high potential vorticity region from the stratosphere coupling to a low-level vortex.

Mid-latitude extratropical cyclogenesis can be reduced to two basic types of mechanisms which initiate and support cyclonic development, "Type A" and "Type B" (Petterssen and Smebye 1971). "Type A" cyclones are associated with a frontal wave, in which the baroclinic region develops prior to the upper-level support from mid-level vorticity advection. The main source of low-level vorticity in the "Type A" case occurs predominately due to the thermal advection and the upper-level troughing that develops in response to the increase in low-level vorticity. The "Type B" case occurs when the low-level cyclone is being conditioned by large-scale orographic forcing. Both of these case types of initiation and maintenance of cyclogenesis occurred in this case study.

The Alps and the Rocky Mountains are ranges that provide a wealth of data sets and analyses (for example Buzzi and Speranza 1983, and Tafferner 1990 and Palmen and Newton 1969). Campaigns such as the Alpine Experiment (ALPEX) which addressed the interactions of airflow, topography and the resultant features from these interactions (Egger 1998, Tafferner and Egger 1990, Alpert et al. 1996) are crucial to developing the diagnostic techniques that individual case studies can utilize in order to weigh the importance of various factors. These large-scale lee cyclogenesis events are largely due to synoptic scale processes in which the upper-level trough amplifies a low-level cyclone that sets up on the lee of topography. Lee cyclogenesis in regions near large mountain ranges is representative of what might happen near smaller mountain ranges, such as near-coastal ranges located along the Eastern Mediterranean Sea coastline.

Almazouri and Awad (2016) broke out cyclogenesis tracks as Northern, Southern, and Eastern Mediterranean Sea regimes. These regimes coincide with clusters of cyclogenetic activity governed by the intersection of the 850 hPa trough and position of the 250 hPa jet. Trigo et al. (2002) detected cyclones by identifying 1000 hPa geopotential height (GHT) minima, and extrapolated "underground" regions by assuming hydrostatic balance. Additionally, Alpert and Neeman (1992) utilized the 10 m wind and 10 m vorticity as a data point to verify the aforementioned method. Furthermore, Alpert and Neeman (1992) examined cold, small-scale Eastern Mediterranean Sea cyclones and noted that occurrences in February coincided with low pressure centers at the northern coast of the Eastern Mediterranean Sea (Alpert et al. 1990), are located 750 km northward of a major jet stream.

Karaca and Dobricic (1997) described meso-beta cyclone formation by the lee of the Taurus Mountains in the Bay of Antalya where topographically forced cyclonic depressions are essentially atmospheric boundary layer phenomena that are too weak to be detected at 850 hPa. The depth of the cyclone in their case study was 1.5 km with a 70 km diameter. They noted that one of the key forcing functions for the low-level cyclonic gyre development, without any upper-level forcing, was the steepness of the Taurus Mountains and flow modification as it hit both Cyprus, with an average elevation of 1950 m, and the Taurus Mountains, with an average elevation of 2000 m.

B. MOTIVATION AND HYPOTHESIS

Weather systems that develop in the Eastern Mediterranean Sea produce rain, wind, and dust storms through many areas in the Middle East. The development of synoptic scale weather systems that occur in regions of complex topography and coastal geography are hard to predict. The dynamical interconnection between synoptic scale features, topography and the ocean system in this complex environment are not well understood or documented in this region.

This case study is aimed at preparing a forecaster, who may have very limited knowledge of this region's weather, to understand the behavior of an upper-level trough that coincides with a polar air outbreak from the Aegean Sea through the Eastern Mediterranean Sea and how these factors combined to produce cyclogenesis in this region. Although the system studied herein resembled a classic mid-latitude baroclinic cyclone on satellite imagery, the complicated interactions with topography on both the mesoscale and the synoptic scale are not well understood. A regional modeling simulation is used to capture small-scale/temporal and dynamic effects to shed light on some of the dependencies of the synoptic scale regional weather to the complexities of low-level orographic forcing.

The goal of this paper, therefore, is to diagnose how an upper-level Black Sea low (UL-BSL) interacted with terrain in the lee of the Middle Taurus Mountains over the Eastern Mediterranean Sea to produce a storm between 17 and 20 February 2015. This system was produced from a 500 hPa trough, and it moved southeast from the Black Sea then transited over the Anatolian Plateau, to continue through the Middle Taurus Mountains, and eventually through the Tigris-Euphrates river valley (TRV-ERV). This 500 hPa cut-off low is examined through interactions of potential vorticity between the boundary-layer and upper troposphere as well as the influence that topography imparts on the temporal evolution of the synoptic and mesoscale structures.

The track of this UL-BSL system, which was directly through the Middle Taurus Mountains, makes this a particularly unique weather system in the region. A case analyzed by Albert and Reisin (1986), which occurred earlier in the winter, described a similar

special path in which the progression of a polar air mass led to an abrupt change in static stability, resulting in a heavy rain event from the sub-tropical cyclone in the Eastern Mediterranean Sea. Figure 1 shows infrared brightness temperatures over the Mediterranean for the case analyzed in this study. The low was emblematic of a mature mid-latitude baroclinic system, based upon the standard Norwegian cyclone model, which seemed to intensify and organize as it traversed the Middle Taurus Mountains. Given the path taken by the upper-level trough and cyclonic cloud structure, the question can be raised as to whether or not the storm underwent a "Type B" initiation of extratropical cyclonic growth as described by Pettersen and Smebye (1971). This type of cyclogenesis requires a surface baroclinic zone and a large-scale orographic influence that shapes the intensity of local and regional impacts lee of the topography. By considering the culmination of cold air retardation, upper-level troughing, warm anomaly lee of the topography, and comma cloud structure that forms in the Eastern Mediterranean Sea, the hypothesis is that synoptic scale lee cyclogenesis occurred lee of the Taurus Mountains over the Northeast Mediterranean Sea.

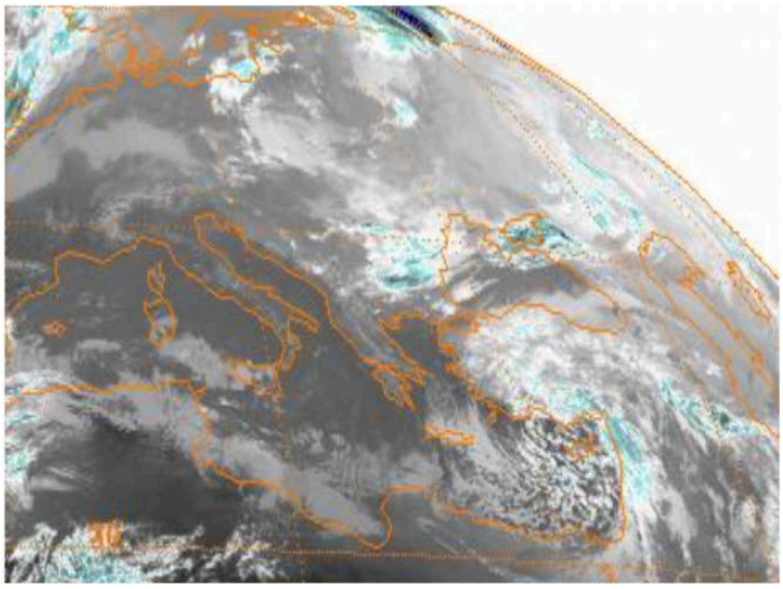

The Meteosat-10 satellite infrared Imagery of the Eastern Mediterranean Sea on at 1500 UTC 19 February 2015 taken from Meteosat 10, displaying a cyclonic comma cloud structure.

Figure 1. Infrared comma cloud. Source: Knapp (2008).

C. OBJECTIVE

Scientists have studied and characterized Eastern Mediterranean Sea cyclone formation extensively, showing these smaller, in some cases, sub-synoptic scale cyclones are common throughout Mediterranean Sea basin. However, there is very little study regarding the lee cyclogenesis in the corridor lee of the Middle Taurus Mountains within the northeastern corner of the Mediterranean Sea. This region, lined by mountainous coastlines, makes the interactions of southeastward transiting upper-level troughs with the topography particularly unique. Characterizing these unique dynamics between the topography and the upper-level trough is the one of the objectives in this study. This study will also show that not only does topography lee of the Middle Taurus Mountains play an integral role on the large-scale, but in the small-scale as well.

The objective of this study is to deduce whether or not synoptic scale cyclogenesis occurred lee of the Middle Taurus Mountains over the Northeast Mediterranean Sea. This research is intended to characterize the dynamics of a particular UL-BSL event and to determine the topographical feedbacks on both synoptic and sub-synoptic scales. This study, unlike previous synoptic scale evaluations of the roles of Middle Taurus Mountains, focuses on transiting upper-level systems, uses a regional model simulation with a sufficient spatial resolution to analyze and detect both large and small-scale features due to topography which may contribute to cyclogenesis.

THIS PAGE INTENTIONALLY LEFT BLANK

II. DATA AND METHODS

This study shows whether or not the position of the upper-level trough axis yields synoptic scale cyclogenesis as it transits the Middle Taurus Mountains. The data and methods used to examine the UL-BSL case study are described in this section. Figure 2 shows the complex topography that the dataset must capture and includes some of the smallest events studied in the region, such as coastal meso-cyclones in the Gulf of Antalya.

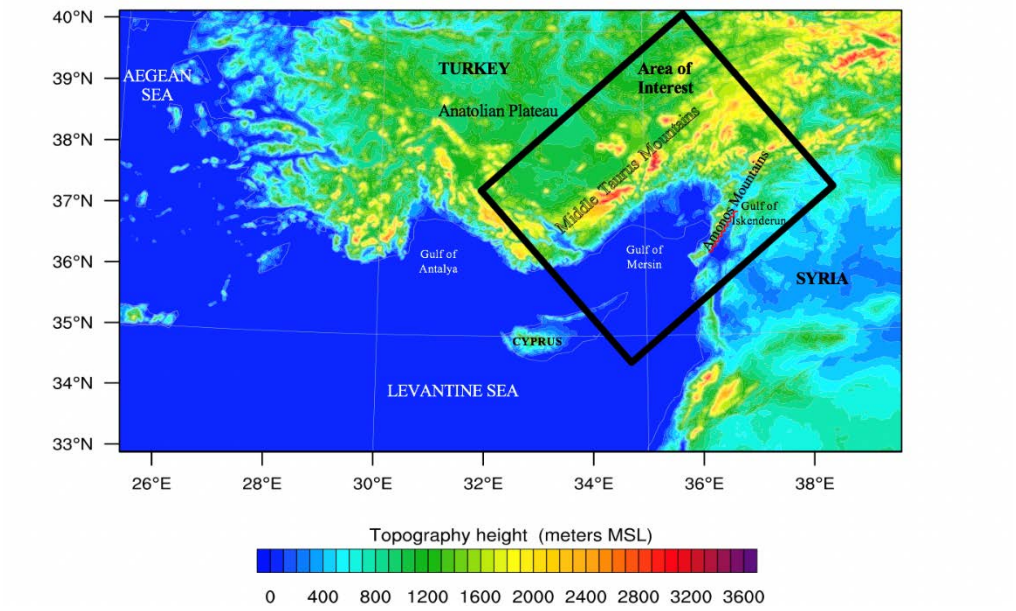

Topography of the Eastern Mediterranean Sea.

Figure 2. Topography (m above mean sea level) with the area of interest for this case study enclosed by the black box

A. CLIMATE FORECASTS SYSTEMS REANALYSIS

The first step taken was to locate surface low pressure regions transiting the Anatolian plateau that deepen lee of the Middle Taurus Mountains. This initial criterion manifested itself through the author's personal observations, as a regional forecaster in the ERV-TRV, of quasi-stationary cyclones that transited from the Black Sea to the Northeast Mediterranean Sea. For the purpose of this study, a coarse resolution, 1° horizontal grid spacing, Climate Forecast Systems Reanalysis (CFSR) data was utilized. The spatial and

temporal domain for the CFSR dataset extended from 20°W to 60°E to 20°N to 55°N and from 1 Mar 2014 to 31 Dec 2018.

The CFSR data set utilizes the Climate Forecast System (CFS), which according to the National Centers for Environmental Information (NCEI), "is a model representing the global interaction between Earth's oceans, land, and atmosphere. Produced by several dozen scientists under guidance from the National Centers for Environmental Prediction (NCEP), this model offers hourly data with a horizontal resolution down to one-half of a degree (approximately 56 km) around Earth for many variables" (NCEI 2019). This one-degree global CFSR data was interrogated using the Gempak Analysis and Rendering Program (GARP) to visually distinguish surface low pressure systems.

B. SATELLITE DATA/OBSERVATIONS

After identification of possible events in which lee cyclogenesis took place, another delineation method was used to sort systems of interest within this study. This was done by selecting a system with sensible weather impacts to the ERV-TRV and satellite structure emblematic of a classic mid-latitude synoptic system. Meteorological Aerodrome Reports (METAR) observations were compiled from the 14 Weather Squadron for possible systems as a means to delineate the systems based on their downstream sensible weather impacts. The geostationary satellite imagery used was derived from data collected by the European Organization for the Exploitation of Meteorological Satellites (EUMETSAT) Meteosat-10 satellite, through the Global International Satellite Cloud Project (ISCCP) B1 Browse System (GIBBS). This archive shows images of the globe at a 3-hour interval from as early as 1980. The Infrared imagery over the Eastern Mediterranean Sea provides a cohesive observational tool between days without running into diurnal transition gaps which arise with visible imagery. Infrared imagery analysis is achieved by comparing cloud temperatures every 3 hours for regions of enhanced cooling which gives a proxy for regions associated with deep convection.

C. WRF

After utilizing the CFSR dataset, a case study was selected for a more detailed analysis. The system transited though the Middle Taurus Mountains over the time period, 0000 UTC 17 to 1800 UTC 20 February 2015. In order to evaluate all synoptic, sub-synoptic, and low-level topographically induced structures the Advanced Research Weather Research and Forecasting (WRF-ARW; Skamarock et al. 2019) model Version 4.1 was integrated over 90 hours. This hourly model output will be used to describe the evolution of this system from this point on. The model output was written hourly in Domains C and D and every 3 hours in Domains A and B (Figure 3). WRF-ARW contained a compressible, non-hydrostatic solver that used terrain following, hybrid sigma-level coordinates. The top of the model was placed at 50 hPa and 41 vertical levels were used. Initial and boundary conditions were from CFSR reanalysis and the outermost boundaries were forced every six hours. No nudging was applied. There was no further additional damping to reduce noise on the simulation aside from numerical damping for extreme vertical velocities, which did not impact normal velocities. Rayleigh damping was also applied near the upper boundary to mitigate gravity wave reflection.

Multiple nested grids, ranging from 54 km to 2 km were centered over the domain of interest. The 6 km domain (Domain C) and the smaller 2 km domain (Domain D) both captured small-scale meso-vortex signatures located lee of the Taurus Mountains. The 6 km was ultimately utilized over the 2 km due to the smoothing effects on the small-scale turbulent features lee of the topography. Figure 3 illustrates the model domain used for this study, and Table 1 outlines the physical parameterizations used.

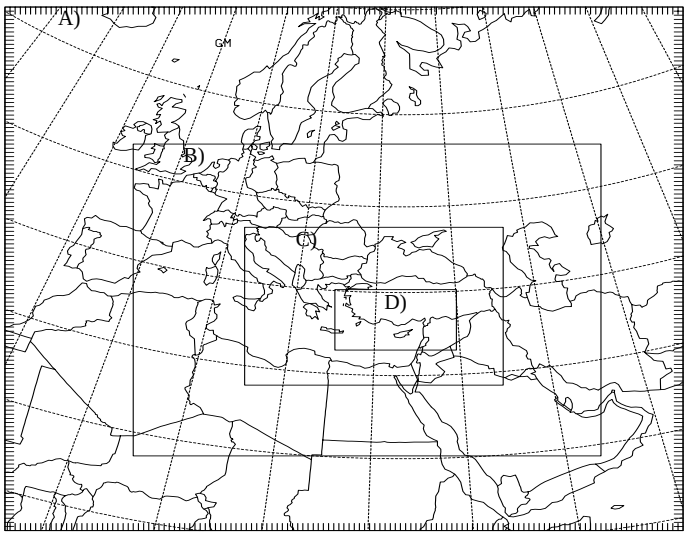

WRF model simulation grid amount / resolution: A) 133 x 127 / 54km, B) 274 x 226 / 18km, C) 454 x 343 / 6km and D) 640 x 394 / 2km.

Figure 3. WRF model simulation domains

Table 1. Model Physics for WRF simulation

Physics	**Scheme**
Microphysics	(WSM3) - (Hong et al. 2004; Hong and Lim 2006; Dudhia 1989)
Longwave Radiation	(RRTM) - (Mlawer et al. 1997)
Shortwave Radiation	(Dudhia) - (Dudhia 1989; Lacis and Hansen 1974; Stephens 1978)
Boundary Layer	(YSU) – (Hong et al. 2006; Hong and Pan 1996; Noh et al. 2003; Jimenez and Dudhia 2012; Lorente-Plazas et al. 2016; Wilson and Fovell 2018)
Surface layer	(Revised MM5) - Jimenez et al. (2012)
Land Surface	(NOAH LSM) – (Chen and Dudhia 2001; Li et al. 2013)
Cumulus scheme	(Kain Fritsch for outermost grid only) Kain 2004; Berg et al. 2013; Berg et al. 2015)

Physical parameterizations used in the WRF simulation for the February 2015 UL-BSL event.

The cyclonic detection method in this study identified regions of anomalous mean sea level pressure and height regions at 1000 hPa similar to the studies conducted be Le Treut and Kalnay (1990) and Alpert et al. (1990). This technique also utilized a unique

approach in quantifying the duration of a cyclone based upon vortex signature via a potential vorticity tower. These cyclonic detection methods were carried out by utilizing the WRF domain with 6 km grid spacing.

Although analyzing the synoptic evolution of cyclones on an isobaric field is common, each individual methodology has its limitations. Hoskins and Hodges (2002) explained that searching for pressure minima leads to overestimates of deep and mature systems and tends to miss small fast-moving systems or cyclones that have best been identified from their local maxima of vorticity. Vorticity maxima are not always shown to be associated with decreases in pressure; therefore, Murray and Simmonds (1991) and Konig et al. (1993) used a combination of both height tendencies and low-level vorticity.

The concentrated regions of positive potential vorticity associated with the evolution of vortices is a critical feature in tracking mesocyclones lee of the Middle Taurus Mountains. These potential vorticity towers serve as tracers through time and space, allowing the trackability in spite of low-level disruptions from topography or other forcing functions.

In Figure 4, the first step is to objectively identify regions of interest, J_{nm}, in which an anomaly associated with a singular cyclone is present. These regions, lee of the Middle Taurus Mountains, are identified based upon anomalous low-level convergence (by analyzing the 925 hPa horizontal wind vectors) and 850 hPa vertical velocities every hour. The bottom two images on Figure 4 represent a single region displayed on the top maps, lee of the Middle Taurus Mountains. In the top left image on Figure 4, the geopotential height map, there is an enclosed isohypse region that is indicated by the red arrow where the low-level signal of the storm can be extracted from the background height anomaly field. In the top right image, the MSLP map, there is no enclosed anomalous isobaric region that can be extracted from the background to depict the location of the storm. So, in this example, at hour 54, only the GHT field can be used to track the duration of this vortex.

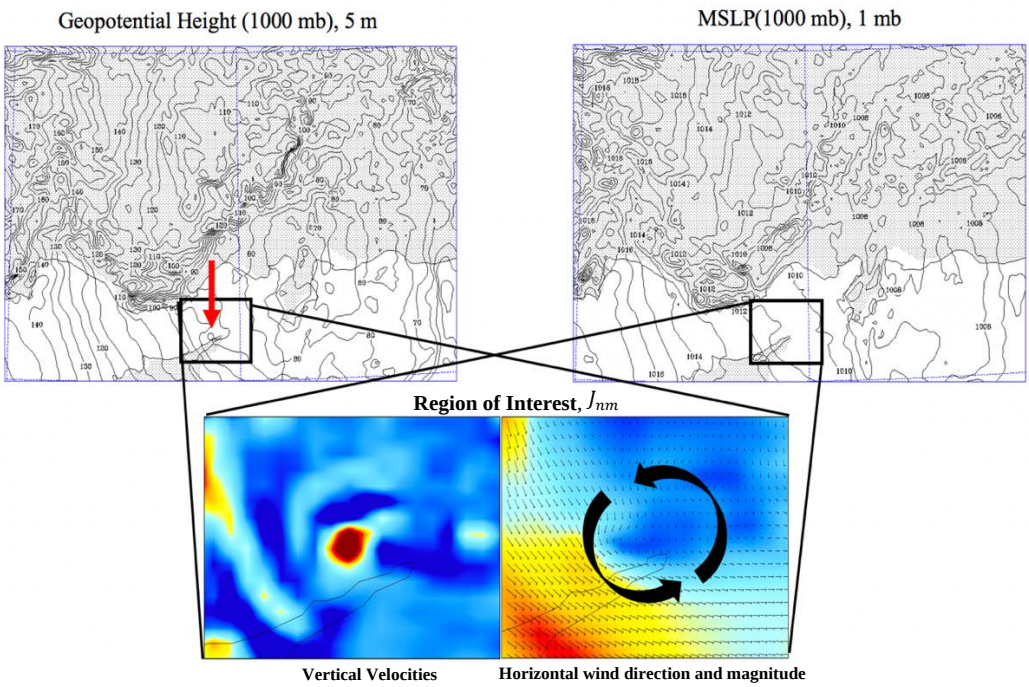

Figure 4 shows an example of hour 54 output, where analyzing vertical velocities (bottom left) and horizontal wind field (bottom right) with a Cyclone B was identified in its progression to the east just off the tip of Cyprus. The cyclone signal is present in the GHT field (top left), but not in the MSLP field.

Figure 4. Determining the regions of interest

To capture GHT anomalies associated with mesoscale gyres approximately 30 km across, these regions, J_{nm}, lee of the Middle Taurus Mountains are analyzed for closed isohypses at 5 m intervals, closed isobars at 1 hPa, and closed regions of potential vorticity at 1 PVU. Table 2 gives the thresholds used to identify these mesoscale gyres. Since the region(s) of interest are subjectively identified, the threshold and the background are the same due to the individual region(s) being chosen with only a single anomaly in the domain. The cross section of potential vorticity through the convective anomaly in each domain was analyzed using a 1 PVU interval, where the top of the potential vorticity tower is the tropopause.

Table 2. Threshold criteria for sub-synoptic cyclogenesis

Threshold Criteria
Closed isobaric region(s) ≤ 1011 hPa
Closed isohypse region(s) (1000 hPa) ≤ 95 m
Closed potential vorticity region(s) ≥ 1 PVU
Regions ≥ 1500 m are masked

A table of threshold criteria to diagnose sub-synoptic cyclogenesis.

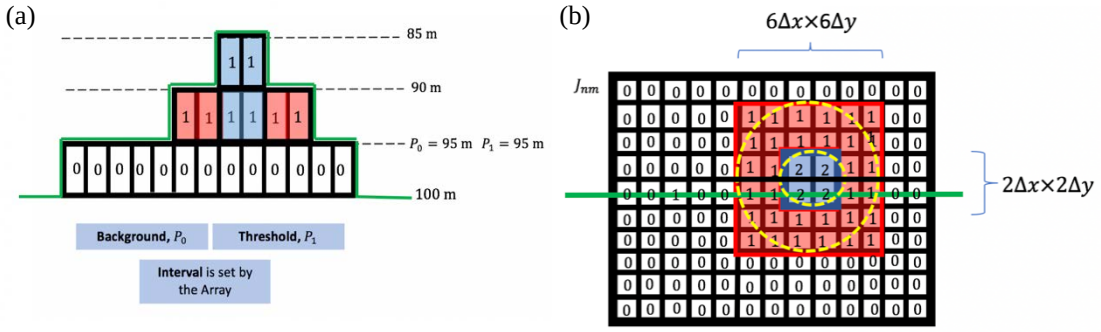

$$\Sigma_n \Sigma_m = ((J_{nm} - P_o)H(J_{nm} - P_1))\Delta_x\Delta_y \qquad \text{(i)}$$

$$A = \Sigma_n \Sigma_m$$

In the cross-section (a) the integral over the region between 95 m and 85 m is equal to the plan view (b) though the green line. In the plan-view the relative area is equal to the sum of the red and blue. The relative area equation (i) expresses both the size and magnitude of the enclosed area of interest (outer yellow dashed circle).

Figure 5. Method for calculating the relative area

This technique of integrating over the region of interest with equation (i) assesses the intensity and duration of the GHT, MSLP, and potential vorticity tower when plotting the relative area values (A) over time-series. Figure 5(a) on the left is a cross-section of the plan-view figure on the right Figure 5(b). The cross-section is an example of determining the GHT of a region where a cyclone is present. The region in this example has only one anomaly. Therefore, the Background P_o and the Threshold P_1 are the same and fitting a square grid over the enclosed region(s) (the dashed yellow circles in Figure 5[b]), shows an assessment of the size and magnitude which is then used to evaluate the intensity that

feature has at the surface (MSLP and GHT [1000 hPa]) or aloft (potential vorticity tower). These calculations can show a signal within the region(s) of interest. If a vortex is present, they can be used to trace the duration and position of the cyclone regardless of the cyclone's stage.

Data analysis in this study is accomplished with a program called VISUAL and Panoply. The VISUAL software, developed by Nuss and Drake (1990), is a meteorological diagnostic tool that allows the user to display and manipulate general meteorological package files (GEMPAK). The VISUAL software uses a graphics kernel system (GKS) primitives and National Center for Atmospheric Research (NCAR) Graphic routines to examine meteorological grids and observations. The NCAR graphics routine is able to ingest the, GEMPAK files from the WRF model from this case and provide a two-dimensional representation of the data. For this study, the VISUAL software was utilized for both for the synoptic over-view and the upper and low-level forcing for lee of the Taurus potential vorticity tower formation.

III. EASTERN MEDITERRANEAN LEE CYCLOGENESIS

A. SYNOPTIC

The mechanisms behind Eastern Mediterranean Sea cyclogenesis, the inter-seasonal variability and unique track distributions have been a thoroughly explored (e.g., Alpert et al. 1990; Trigo et al. 2002; Flocas et al. 2010; Almazouri and Awad 2016). The ability to accurately assess cyclogenesis in this region is paramount to determine the climatic feedbacks and precipitation that these systems can impart (Flocas et al. 2010, Alpert et al. 1990) and also aid in expounding upon the best cyclone identification techniques covered by (Trigo 2006; Alpert and Neeman 1992; Alpert et al. 1990; Trigo et al. 2002; Flocas et al. 2010; Almazouri and Awad 2016).

Numerous studies on cyclogenesis in and around the Mediterranean basin have identified various geographical factors that play critical roles in the evolution of these systems. However, research on cyclogenesis specifically in the lee of the Middle Taurus Mountains, is limited. The focus of this study is to develop an understanding of UL-BSL events interacting with the Middle Taurus Mountains. Alpert and Reisin (1986) and Karaca and Dobricic (1997) both cite the orographic effects of the Taurus Mountains in specific, rare, or unusual cases of mesoscale cyclones. However, they show no evidence in which lee cyclogenesis occurred on the synoptic scale.

Analyzing the CFSR reanalysis data set for MSLP anomalies and 500 mb troughs, at 4 hPa and 20 m interval, showed no closed isobaric regions were observed to form lee of the Taurus Mountains as an upper-level trough transited through the Eastern Mediterranean. Thus, only the upper-level forcing, found present in this region, is crucial in the genesis of the large-scale cyclonic structure. By examining just 500 hPa cut-off upper-level lows, transiting from the Black Sea to the Taurus Mountains, 25 events of interest were identified.

Four distinct upper-level, cut-off lows were then chosen as shown in Figure 6. The four cases were then delineated by first the track from the Black Sea to the Taurus Mountains, then having a sensible weather impacts on the Tigris-Euphrates River Valley (ERV-TRV), and lastly by having an infrared satellite signature emblematic of a classic mid-latitude system (Figure 1). The system which transited the region mid-February 2015 best fit this profile. Figure 7 shows the infrared imagery of the four events chosen for further analysis. In both images a and b there is a distinct cyclonic cloud feature over the Bay of Mersin, indicative of what would otherwise be analyzed as a mid-latitude cyclone.

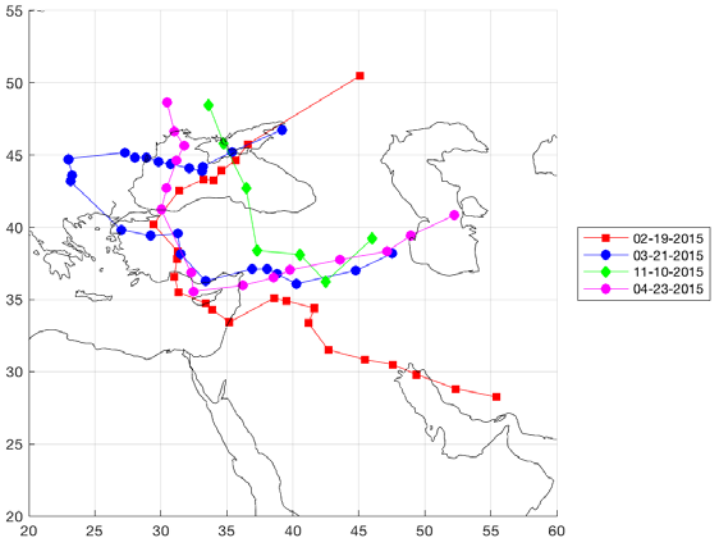

A plot of 500 hPa GHT tracks of four UL-BSL events that met the general criteria for locating a system that met: The Black Sea to Taurus Mountains track, satellite imagery (cyclonic), and downstream observations.

Figure 6. 500 hPa GHT tracks of UL-BSL events

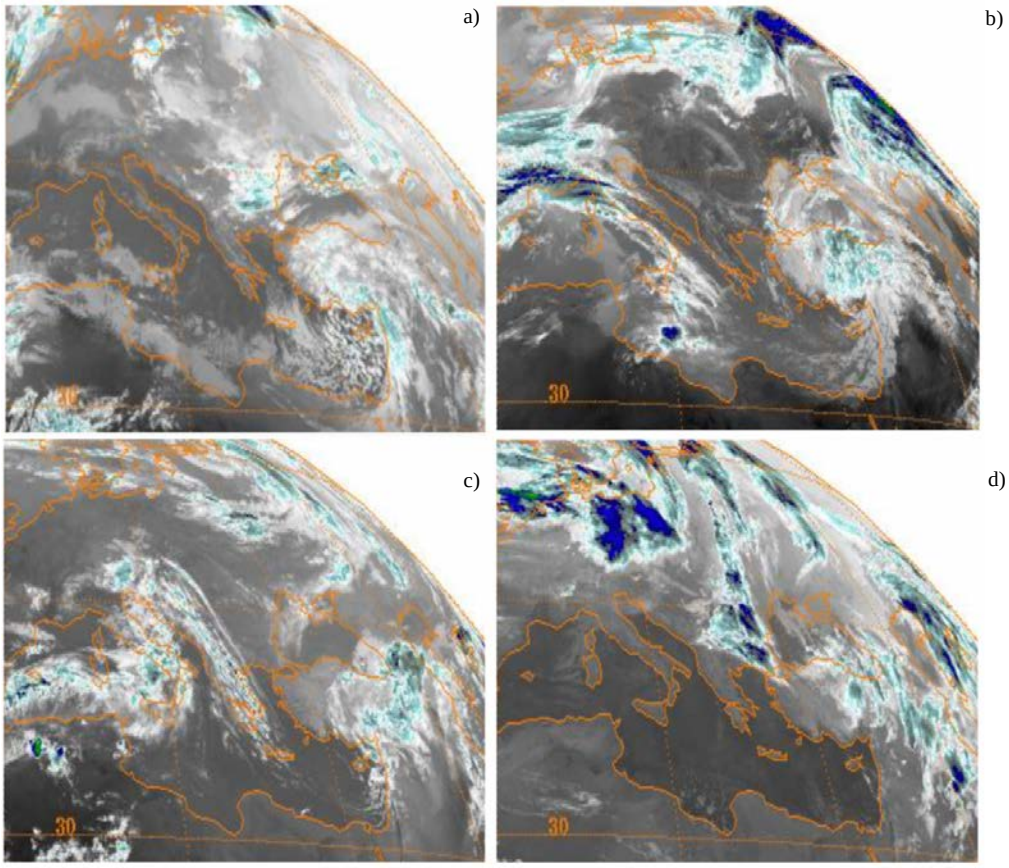

The Meteosat-10 satellite infrared imagery of a) 19 February 2015 b) 21 March 2015 c) 23 April 2015 d) 10 Nov 2015 noting the both the cyclonic structure of a and b.

Figure 7. Infrared imagery of four cyclones over the Middle Taurus Mountains. Source: Knapp (2008).

B. SATELLITE DATA AND OBSERVATIONS

It can be observed in Figure 8 that a cyclonically rotating cloud shield is centered of the Northeastern Mediterranean Sea. A frontal feature is evident on the eastern most Mediterranean Sea shore that extends from the Gulf of Mersin south toward the Gulf of Suez (hour 60 image). There also appears to be a deformation region along the Northern Anatolian Plateau from the 48 to 60-hour period, as well and a dry slot entering in from the northwest observed through the entire period consistent with the high potential vorticity air associated with the upper-level trough. These satellite structures play a critical role in first identifying the event type impacting the region. The question then becomes whether or not this structure is indicative of a lee cyclogenesis event or is this a unique occurrence of a

barotropic upper-level system forced topographically to take on the baroclinic-like structure observed by satellite. During the 60- and 72-hour time frames, the structure of the system had a baroclinic likeness to the structure observed in satellite imagery of a mid-latitude baroclinic system.

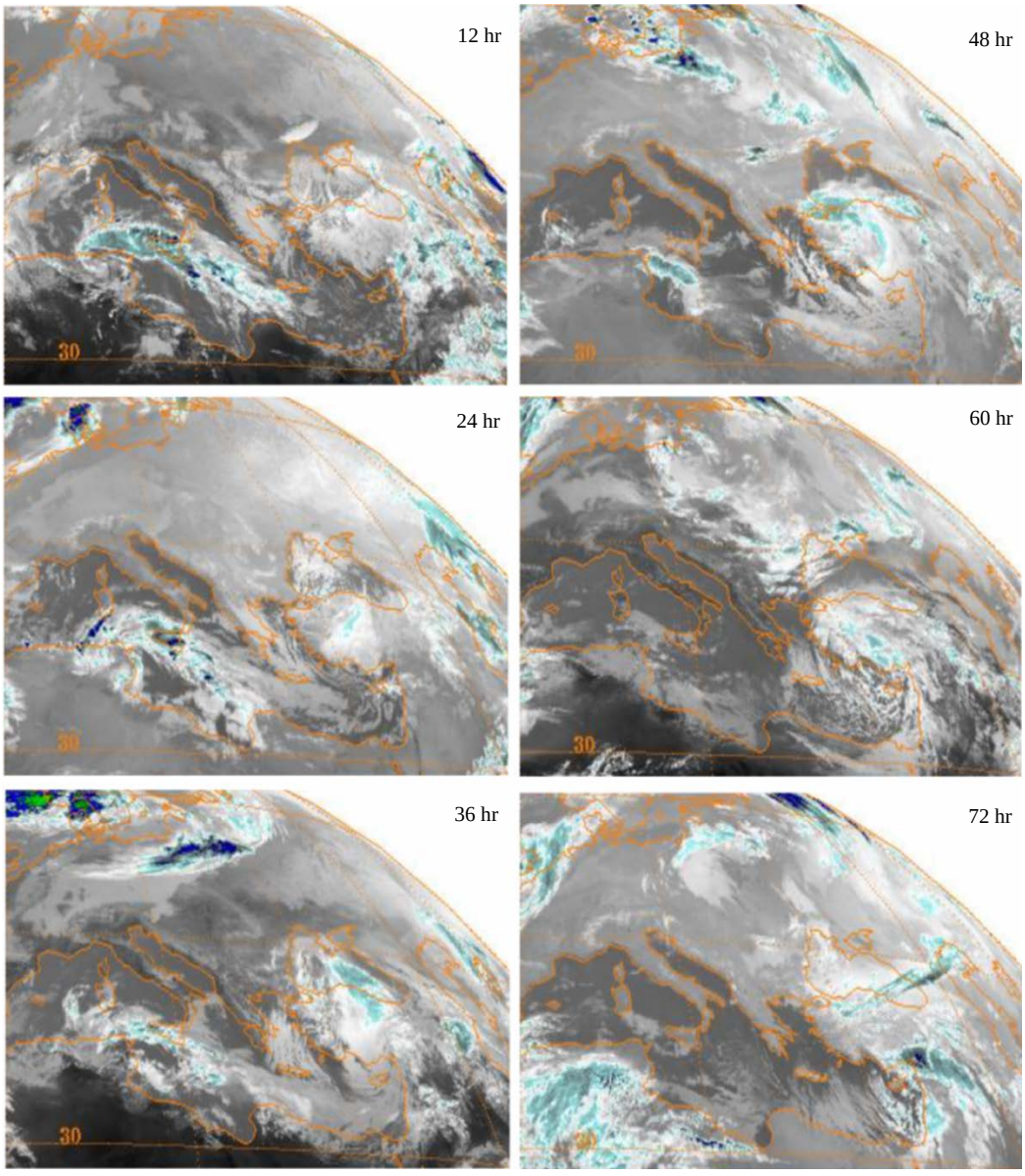

The Meteosat-10 satellite infrared brightness temperatures show the 3-hourly progression of the upper-level system as it progressed from 1200 UTC 17 February (hour 12) to 0000 UTC 20 February 2015 (hour 72).

Figure 8. Infrared satellite imagery for February 2015 storm. Source: Knapp (2008).

Figure 9 is a baroclinic diagnostic of the system at 1500 UTC 19 February 2019. It is evident that over the Northeastern Mediterranean Sea this system shares the same characteristics of a typical mid-latitude cyclone. Diagnosing the cyclonic cloud structure in Figure 9 shows the following structures: (1) Cold and dry, polar air mass is pushing out through the Eastern Mediterranean Sea from the Aegean Sea; (2) Deformation region, a compressed/shield-like structure in the clouds over the Anatolian is similar to the polar front jet compressing the 700 hPa moist conveyor in the northwestern periphery of the cyclone; (3) The placement of the warm front is with a band of clouds north of the apparent surface low (4); (5) The cold front occurs where a band of clouds has formed in higher terrain along the eastern edge of the Mediterranean Sea. (6) The TROWAL (trough of warm air aloft) is in what is the leading edge of the cold front, in the moist warm air to the South.

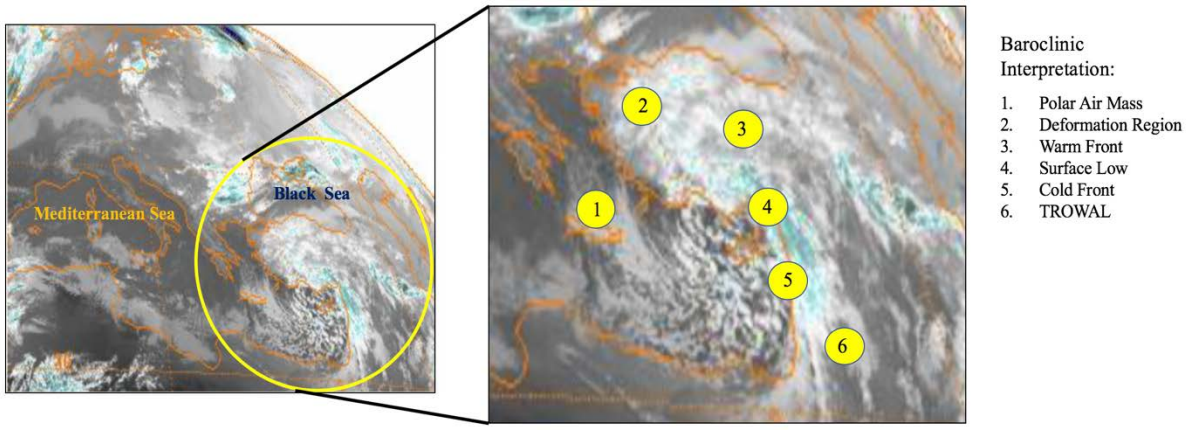

The Meteosat-10 satellite infrared shows the baroclinic-like features of the storm at 1500 UTC 19 2015.

Figure 9. Baroclinic features imagery diagnostic.
Source: Knapp (2008).

Table 3 shows a sample of the downstream effects which occurred with respect to this February 2015 storm. Rain in Northern Syria and Central Iraq and thunderstorms, rain, and snow in Northern Iraq are events that can all be tied to mission limiting thresholds. These sensible weather impacts are critical shaping factors of the downstream areas of operations (AOs), which highlight the importance of understanding the intricacies of these UL-BSL events as they transit into the region.

Table 3. Downstream sensible weather impacts from the UL-BSL

Sensible Weather (ERV-TRV)		Precipataiton Window		
Location/ICAO	Elevation (meters)	Begin Time, Precipitation Type	End Time, Precipitation Type	Sensible weather in Window
Baghdad International Airport/ORBI	34.74m	(02/19/1700Z), -RA	(02/21/1530Z), -RA	RA,SHRA,BR,
Erbil International Airport/ORER	408.73m	(02/19/1300Z), -TSSHRA	(02/20/2200Z), -RA	TSSHRA,RA
Qamishlo International Airport/OSKL	451.1m	(02/19/0500Z), RA	(02/20/1100Z), RA	RA,BR
Sulaymaniyah International Airport/ORSU	760.17m	(02/20/0100Z), TSSHRA	(02/21/1200Z), -RABR	TSSHRA,RA,SN,BR

A table of locations in Syria and Iraq impacted by the 19 February 2015 UL-BSL.

C. SYNOPTIC EVALUATION

The UL-BSL system that occurred between 2100 UTC 17 – 0000 UTC 20 February 2015 was chosen for a detailed analysis. The unique synoptic pattern and complexity of the geography in and around the Mediterranean Sea determines, to a great extent, the location of cyclogenetic regions (Trigo et al. 2002). Figure 10 shows that the path which the upper-level trough and associated polar air mass took as it transited the Aegean Sea. The polar air swept south, fanning out into the Northern Levantine Sea, bounded at the Northern extent by the Taurus Mountains. Meanwhile the upper-level trough and associated cold dome continued to circumnavigate the terrain through the Anatolian Plateau until piling along the lee side of the Taurus Mountains. This retardation of cold air by the Taurus Mountains along the windward face is critical for lee wave formation (Pettersen and Smebye 1971). The right graph on Figure 10 shows the 500 hPa trough deeping between the 40 to 60-hour period as it moved over the Taurus mountains.

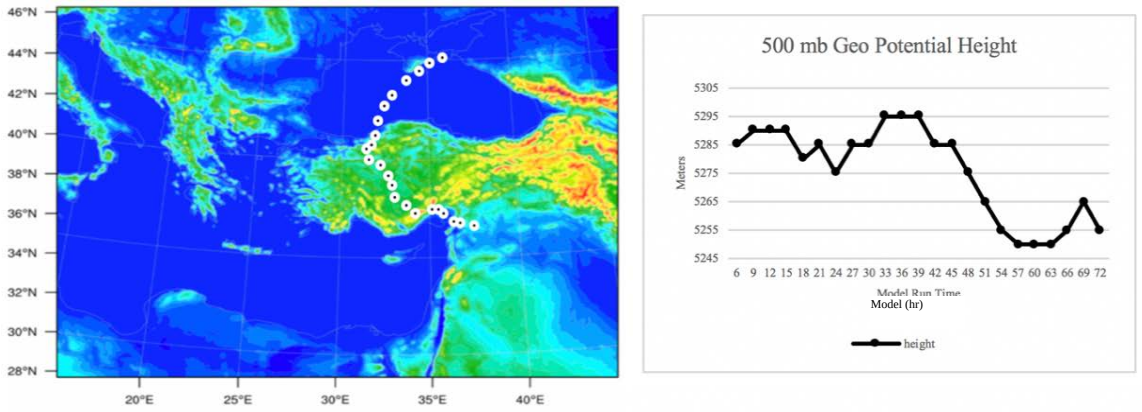

The third WRF nest topographical map with 500 hPa geopotential height centers plotted white circles showing the progression of the upper-level low from the northern most edge of the Black Sea to through the Middle Taurus Mountains.

Figure 10. 500 hPa track of February 2015 UL-BSL event

Figure 10 reflects the upper-level system's descent from the Black Sea, over the Anatolian Plateau and across the Middle Taurus Mountains. The blue dot on Figure 11 shows the location of the Bay of Mersin in the lee of the Middle Taurus Mountains. The upper-level trough descends southward from the 12-24-hour period. Then at hour 36 the trough becomes cut-off only to re-join the following upper-level trough on hour 48. From the 60-72-hour period the "comma cloud" structure over the Northeastern Mediterranean Sea and the upper-level low were directly over the region.

Through the 12-72-hour period high pressure prevailed over the region inducing a lee trough with an 8 hPa pressure gradient developing along the Middle Taurus Mountains (Figure 12). The 500 hPa low became cut-off from the parent upper-level trough at 1200 UTC 18 February, only then to rejoin the subsequent upper-level trough, being finally ejected with the high building in from the west (Figure 11).

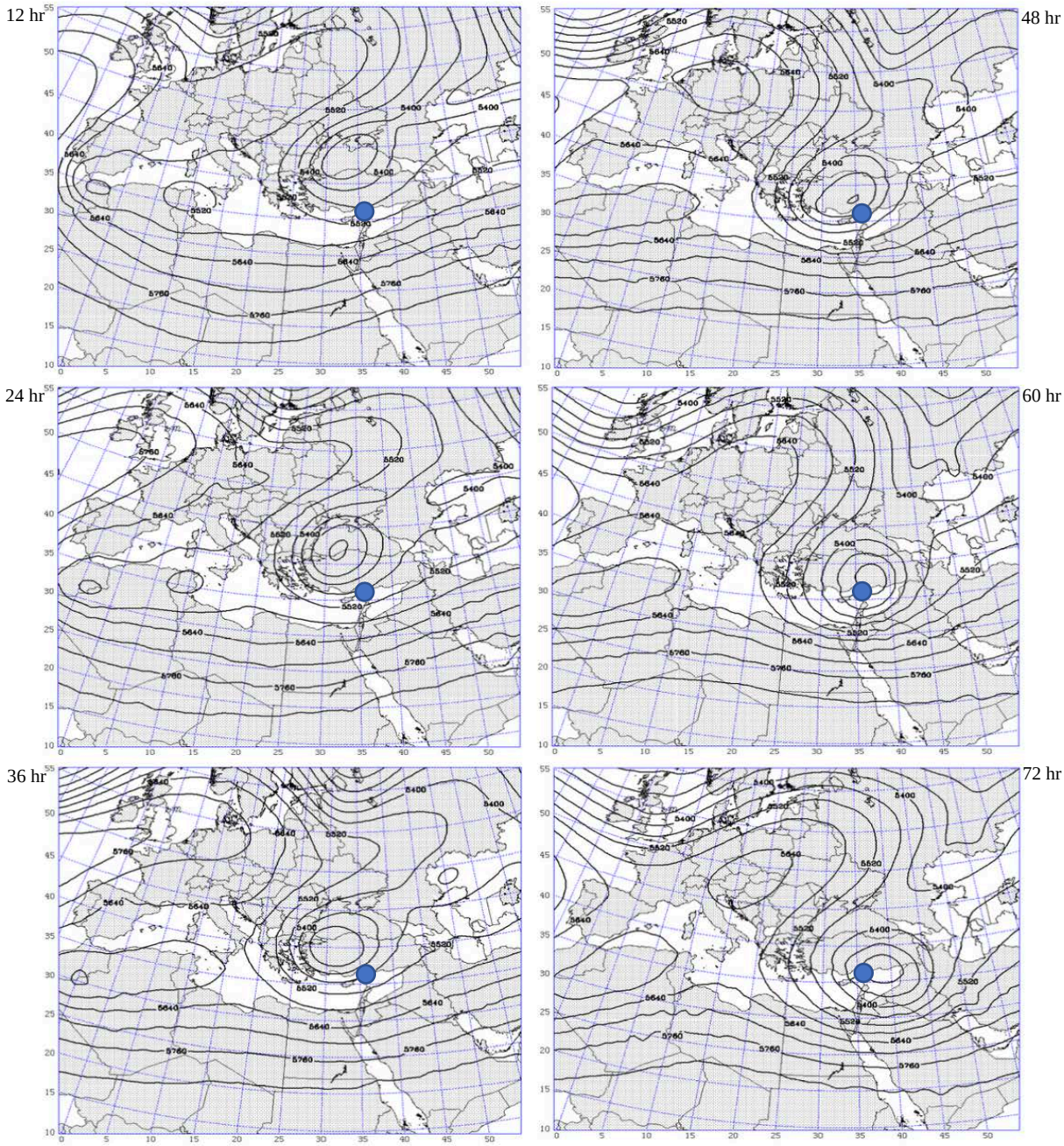

16 km WRF simulation 500 hPa geopotential height (black lines) showing upper-level low becoming cut-off by the hour 36 to then re-join the subsequent upper-level trough by the hour 48. The upper-level trough is shown in the proximity to the lee of the Middle Taurus Mountains, represented as the blue circle. At the hour 60 the upper-level low is directly over head of the Middle Taurus Mountains.

Figure 11. Synoptic 500 hPa GHT, cut-off low

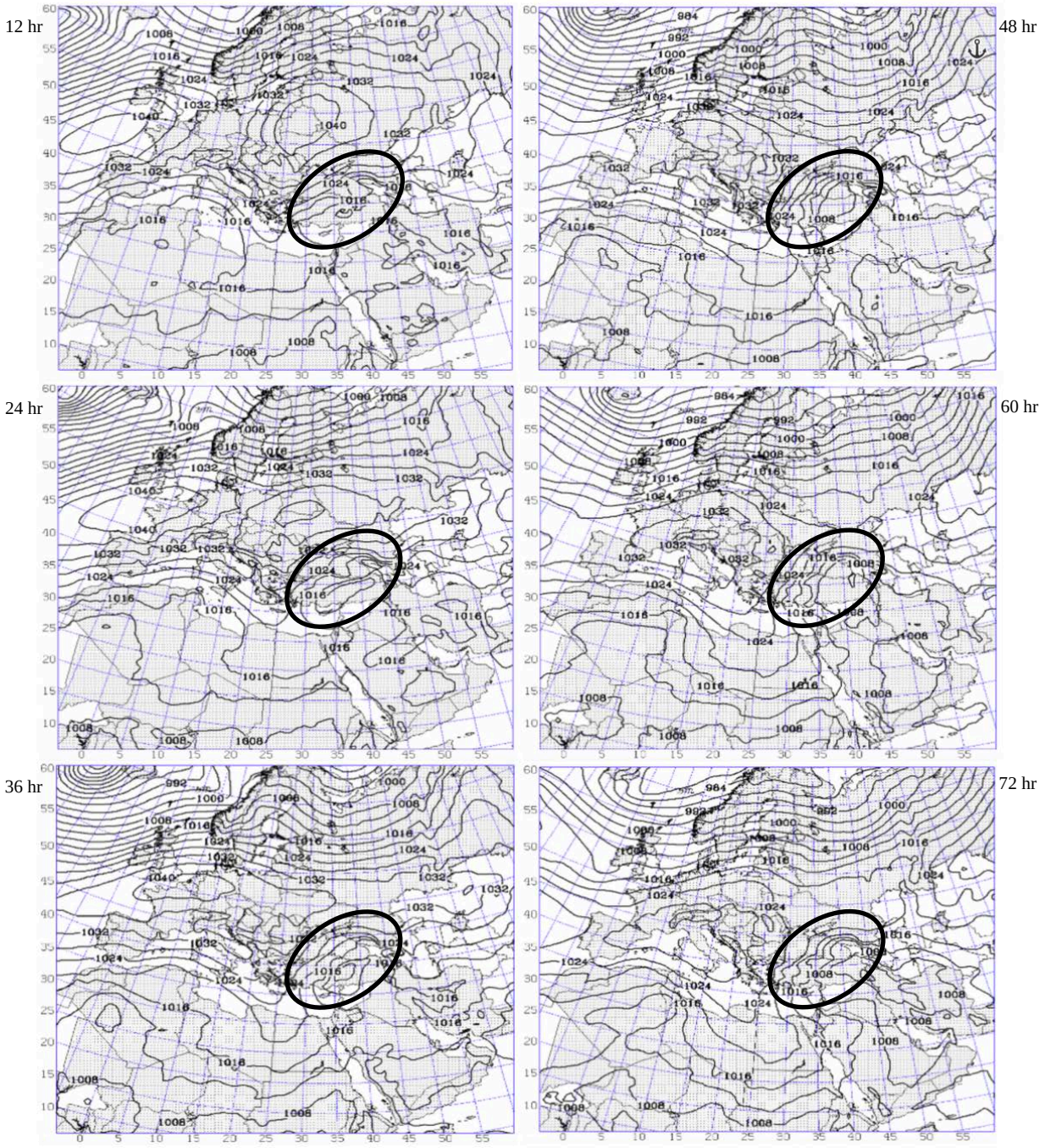

16 km WRF simulation of MSLP (black lines) showing a broad region of low MSLP developing along the lee of the Taurus Mountains in the black oval. At hour 36 there is a 1016 hPa low pressure region along the Middle Taurus Mountains.

Figure 12. Synoptic MSLP analysis

Honing in on the 1200 UTC 19 February time frame, during which time the satellite structure is baroclinic-like, MSLP and GHT at 500 hPa is further examined in Figure 13. During the period in which the baroclinic-like cloud structure was located over the Middle Taurus Mountains, a broad region of low pressure existed over the Taurus Mountains, indicative of topographically forced low-level convergence. The 500 hPa trough was directly over the Middle Taurus Mountains indicating a barotropic environment rather than a baroclinic environment.

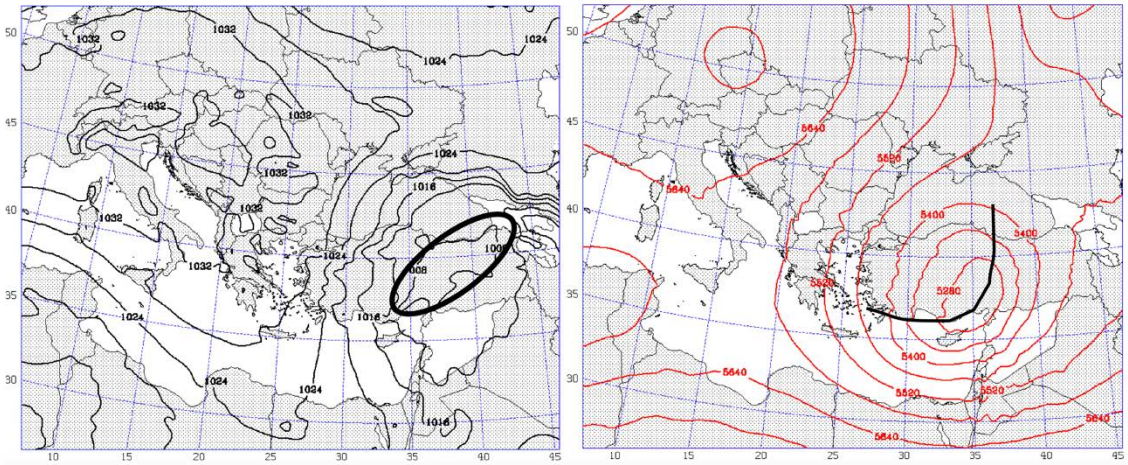

16 km WRF simulation MSLP (black lines) (left) and 500 hPa geopotential height (red lines) (right) at hour 54 showing a broad region of low pressure over the Taurus Mountains along in a very barotropic setting with the 500 hPa trough directly over the Middle Taurus Mountains.

Figure 13. Isobaric analysis

Looking at the red arrows on Figure 14 and following the 296 K isentropic surface, moist upglide over terrain is observed as the specific humidity shows parcels that follow a cyclonic trajectory around the upper-level low. The bulk of the moisture is farther to the east and relatively dry air resides lee of the Middle Taurus Mountains. This localized region of dry air is a critical observation in understanding that the cusp in the cloud structure, where generally a surface low would be present with adjoining fronts, is merely a region over water void of low-level forcing of moisture over topography.

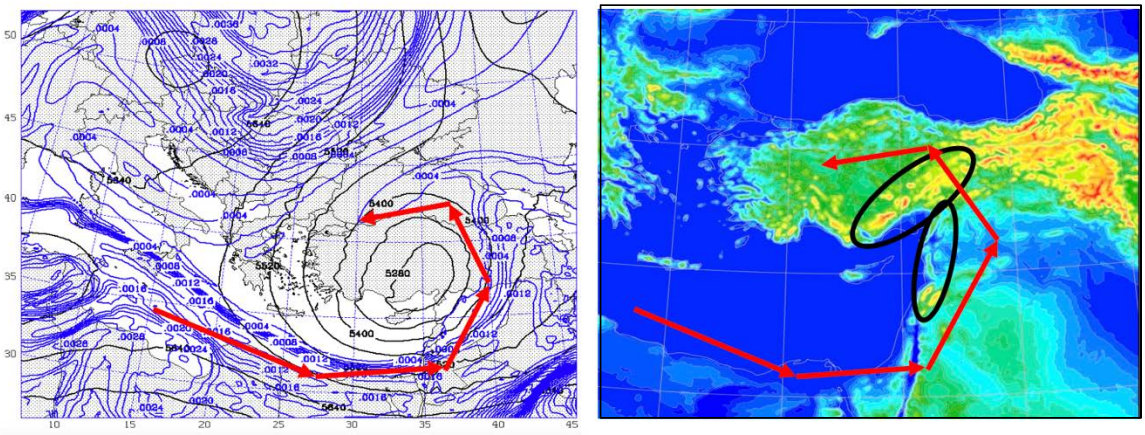

16 km WRF simulation specific humidity (blue lines) on the 296 K isentropic surface at hour 54. The red arrows show the cyclonic motion of the moisture field advecting over the Taurus Mountains.

Figure 14. Isentropic analysis

The position of the jet and the Bay of Mersin are shown in Figure 15 and summarized in Figure 16. During the 12-36-hour period, by measuring the distance of the 850 hPa trough, co-located with the Middle Taurus Mountains, to a major jet max to the south is outside the 750 km proximity that Alpert and Neeman (1990) deemed as one of the characteristics crucial to the formation of cold small-scale cyclones over the Eastern Mediterranean Sea. The proximity of the jet is within the 750 km range to the Bay of Mersin during the 48 -72-hour period. In this period, although it does meet the distance criteria, the 500 hPa trough is co-located with the 850 hPa trough. This equivilant barotopic structure developes due to pooling of cold air from the surface to 900 hPa, resulting in the deepening of the upper-level low between the Middle Taurus Mountains and the Amonos Mountains.

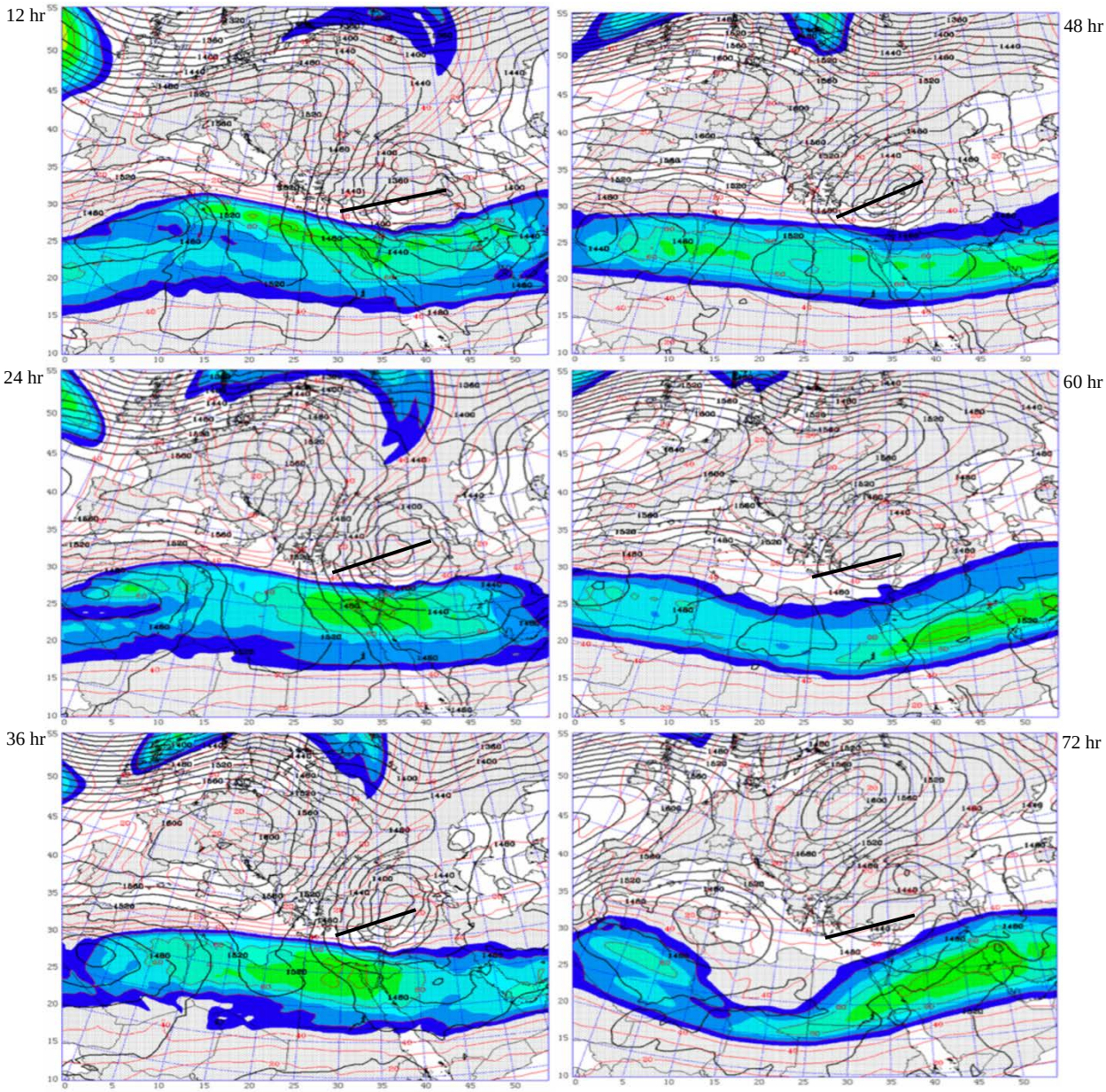

16 km WRF simulation showing the proximity of the 850 hPa geopotential height (black lines), co-located with the Middle Taurus Mountains, to the 250 hPa jet (color fill). During the 12-36-hour period, the position of the jet is outside the 750 km proximity of the Bay of Mersin. During the 48-72-hour period, the proximity between the jet and the Bay of Mersin is less the 750 km.

Figure 15. Bay of Mersin and 250 hPa jet

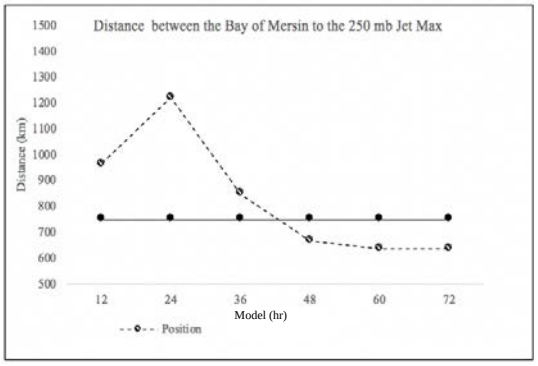

16 km WRF simulation graph showing the proximity (dashed line) of the 250 hPa jet to the Bay of Mersin. The solid line represents the 750 km vicinity threshold of jet support for cyclogenesis (Alpert and Neeman, 1990).

Figure 16. Jet support for cyclogenesis

Table 4 shows when evaluating this system based upon established Eastern Mediterranean Sea criteria it is clear that this system does not meet all the requirements for a synoptic scale cyclone. This system met the duration ≥ 24 hours, the upper-level trough was present 48+ hours, but the criteria that the low-pressure center was in a region ≤ 1500 m, was not met. So, although this cyclone did not meet all of the thresholds for synoptic scale cyclogenesis, there exists multiple sub-synoptic vortices lee of the Middle Taurus Mountains due to the position and track of the upper-level trough, which will be explored in the next section.

Table 4. Eastern Mediterranean Sea synoptic criteria vs. 19 February 2015 event

Eastern Mediterranean Sea synoptic scale Criteria	**19 February Event**
Minimum duration ≥ 24 hr	Met criteria, Upper-level support was greater than 24 hr
Horizontal scale 200+ km	Met criteria, ~450 km
Pressure center ≤750 km northward of a major jet	Met criteria, 36 hr and beyond
Maximum MSLP ≤1010 hPa	Did not meet, no clear minimum
Elevation in which they occur ≤ 1500 m	Did not meet, pressure minima occur above 1500 m

Alpert et al., (1990), Trigo (2005), Alpert and Nemman (1992), Karaca and Dobricic (1997), Flocas et al., (2010)

A table comparing the diagnostic results from the 19 February 2015 system to Eastern Mediterranean Sea synoptic scale criteria.

D. MESOSCALE

One of the key issues to arise within the methodology of current cyclone discrimination is that the algorithms are not fine-tuned to high resolution, low frequency events. Current coarse resolution datasets employed to locate and track cyclogenesis cannot capture smaller scale cyclones and secondary cyclones imbedded in complex systems (Trigo 2006).

Attempts to construct objective definitions of small, cold-core cyclones that fit the common classical definitions have been identified. Definitions include cyclones based both on the relative vorticity and geopotential height fields, concluding that cold small-scale cyclones:

> (i) occur mainly in February with their low center at the Northern Coast of the eastern Mediterranean Sea, (Alpert et al., 1990) 750 km northward of a major jet stream (ii) Their central vorticity attains high values relative to cyclones with similar horizontal scale (iii) The low tropospheric (1000–850 hPa) static stability is close to the total average of ~7.5 K km^-1, a value which seems to result from the exact average between the moist and dry adiabatic lapse rates (iv) They are in general slightly more baroclinic than an average eastern Mediterranean Sea cyclone. At the same time, the latent heat fluxes are also larger than average, indicating the importance of local convection. (Alpert and Neeman 1992)

This case study of the UL-BSL event is similar to the Genoa and Colorado low formation, which embodies a two-phase process of lee cyclogenesis. These phases include an advancing upper-level trough, topographically forced cold damming along the windward (Northern) side of the Middle Taurus Mountains, creating an initial temperature and pressure gradient necessary for deep cyclogenesis and the precursor low-level mesoscale vortex generation (Figure 17). Unlike the aforementioned “typical” events, lee of the Middle Taurus Mountains is a relatively small, well mixed region, dominated by gap flows stabilizing and shunting the organization of a low-level vortices. It can be observed that many of these low-level circulations, topographically generated, arise to the lee of the Middle Taurus Mountains and are heavily sheared and advected from a series of gap winds that dominate boundary layer interactions up to 400 hPa.

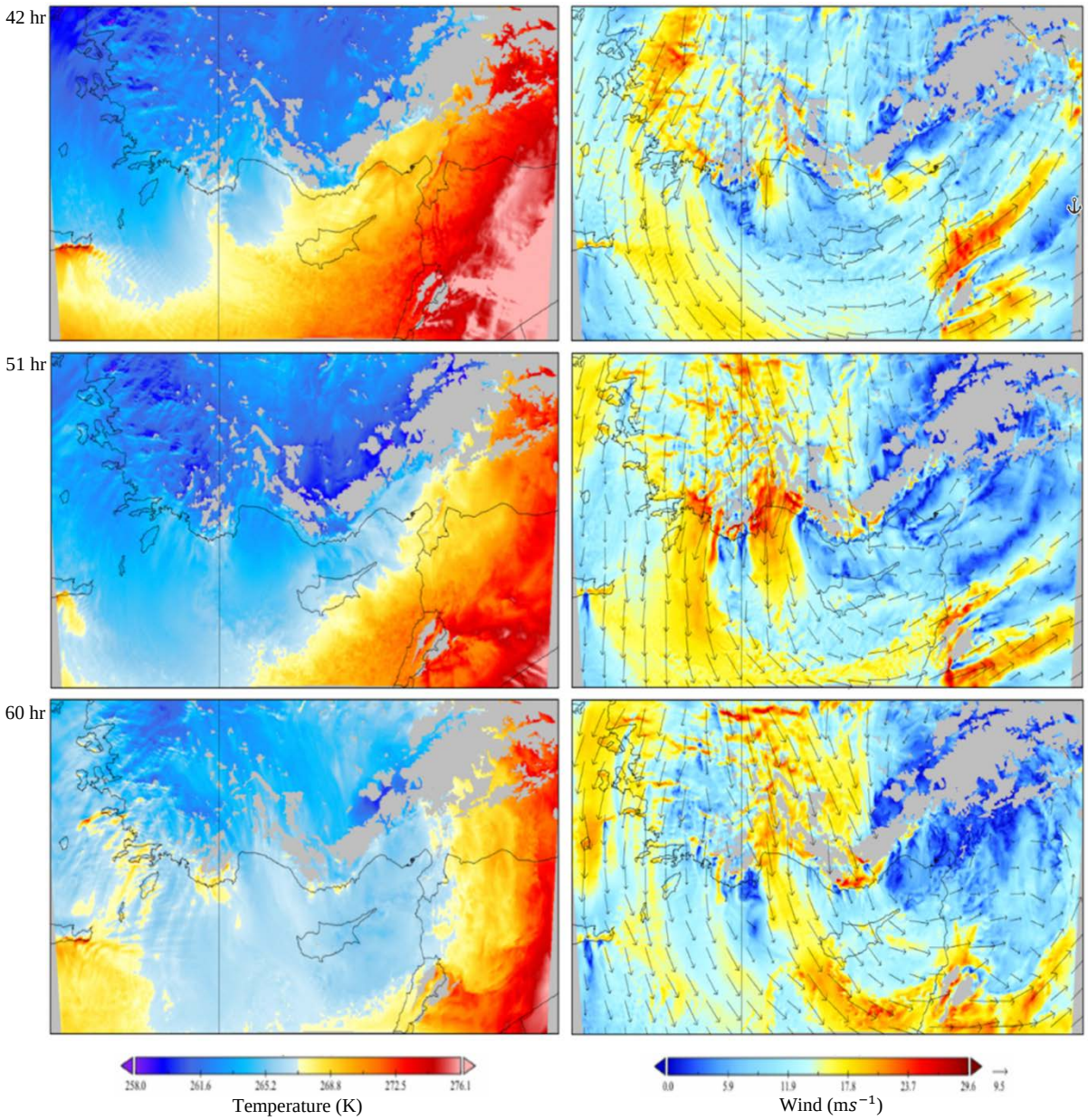

18 km WRF 850 hPa Temperature and Wind field with vectors showing the air retardation along the Taurus Mountains. Hour 42 shows the warm anomaly lee of the Middle Taurus Mountains. Hours 51 and 60 show low-level mixing lee across the Eastern Mediterranean Sea. The 42-60-hour period shows broad cyclonic circulation as the wind funnels through the gap, to the North of Cyprus then northeastward creating a depression in the wind field over the higher terrain farther to the northeast.

Figure 17. Cold air damming

Two notable events occurred lee of the Taurus Mountains over the Northeastern Mediterranean Sea, one transpiring on the 0600 UTC 18 February 2015 (Cyclone A), and the other transpiring on 1200 UTC 19 February 2015 (Cyclone B)(Figure 18). What makes these two events unique to one another is the earlier event, Cyclone A, developed in a baroclinic environment, whereas the later event Cyclone B, developed in a barotropic environment. Both events were sub-synoptic systems having only localized MLSP anomalies on the order of 2 hPa, and maxima wind fields at 925 hPa of 30-50 km. In both cases an orographic induced gyre in the Bay of Mersin initiated low-level vorticity generation.

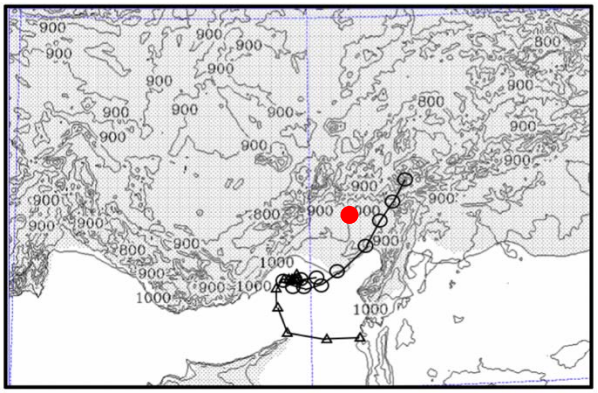

Both Cyclone A (circle) and Cyclone B (triangle) are plotted at one-hour intervals, originating in the Bay of Mersin (red circle).

Figure 18. Cyclone (A) and (B) tracks

Despite a post frontal, statically stable environment, these gyres that manifested at the lower boundary due to orographic influences became coupled with the upper troposphere, resulting in a redistribution of potential vorticity. Figure 19 is a cross section showing an example of the resulting potential vorticity towers for both cyclones (A) and (B).

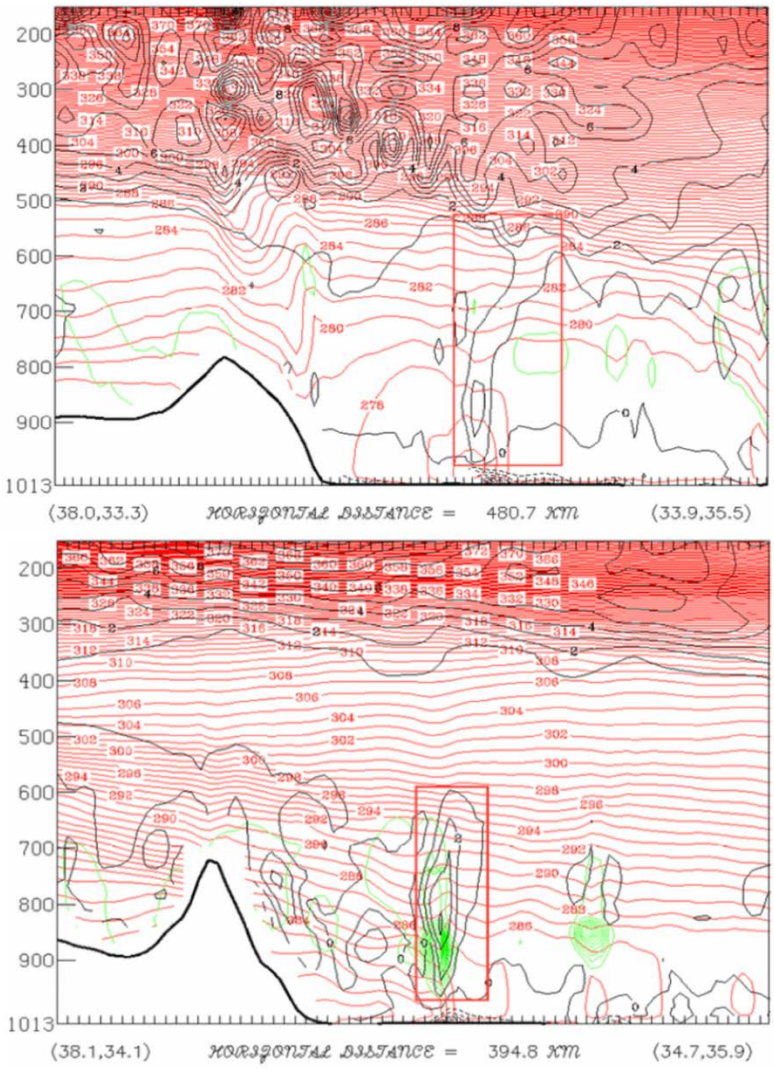

6km WRF cross section of Cyclone A (top) and Cyclone B (bottom) showing potential vorticity towers in the (red box), taken at 0600 UTC 18 February (top) and 1200 UTC 19 February 2015 (bottom). The red lines are potential temperature, at 1 K interval. The black lines are potential vorticity, at a 1 PVU interval and the green lines are cloud water, at a .0005 gm^{-3}interval.

Figure 19. Potential vorticity towers

E. CYCLONE (A)

Cyclone A developed during the period of time in which the surface cold front rushed along the lee of the Taurus Mountains created a thermal wave that traveled into the Northeastern Mediterranean Sea. This wave, created ahead of the surface front, never

amplified due to the gap winds through the Göksu River valley on the west side of the Bay of Mersin and gap winds through valley of Çakıt on the northern shore of the Bay of Mersin. These series of large valleys along the Southern Turkish coast created a highly mixed boundary region out ahead of the surface front, shunting the prospects of low-level vortex organization. Although the main thermal wave was never amplified, when the cold front moved into the north-easternmost corner of the Mediterranean Sea, 0600 UTC 18 February, cyclogenesis ensued with a topographically induced gyre. This gyre, along the lee side of the Middle Taurus Mountains, organized in Bay of Mersin and utilized the potential vorticity associated with the upper-level trough, as the 500 hPa vorticity maxima pushed East over the region (Figure 20). The cyclonic region then moved over the junction of the Middle Taurus Mountains and the Amonos Mountains through the Armenian Bay by 0200 UTC 18 February.

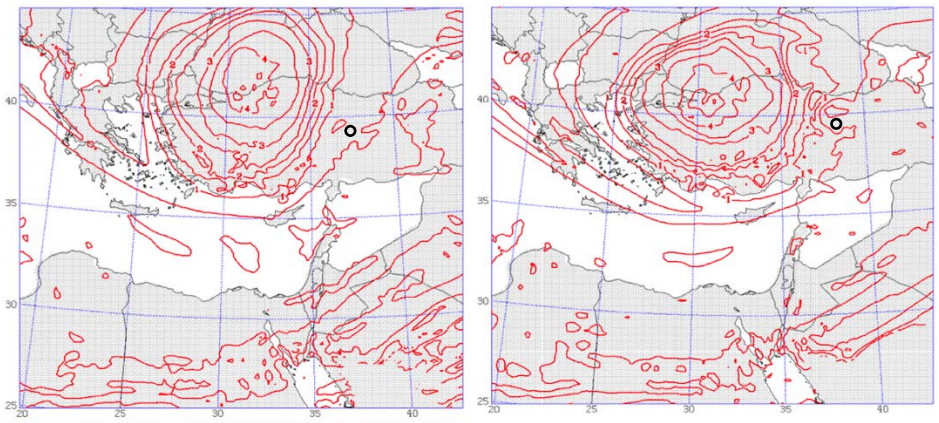

18km WRF 296 K isentropes (red line) at 0300 (left) and 0900 UTC (right) 18 February and the location of Cyclone A (black dot), show region of potential vorticity associated with the upper-level trough track to the south-southeast.

Figure 20. Upper-level trough on a 296 K potential vorticity surface, Cyclone A

The cross section in Figure 19 (bottom) is taken along an NW to SE vertical plane, orthogonal to the Middle Taurus Mountains. The slope of the isentropes, indicate that the environment is baroclinic in nature, and follows a more Type B case of cyclogenesis (Pettersen and Smebye 1971). This Type B case develops with a pre-existing upper-level trough over a region characterized by strong leading positive vorticity advection, and in

this occurrence, a low-level vorticity anomaly generated by topographical forcing out ahead. This cross section also depicts cold air damming is present along the wind-ward side of the Middle Taurus Mountains and a relatively warm anomaly exists, consistent with the warm-air advection ahead of the 850 hPa trough.

F. CYCLONE (B)

Cyclone B developed in a post frontal, conditionally unstable, equivalent barotropic environment, where the center of circulation at the 500 hPa level extends to the surface lee of the Middle Taurus Mountains. Figure 21 shows that the potential vorticity maximum is directly over the region of that Cyclone B. The cross section in Figure 19 (top) indicates a tropospheric fold, in which the base of the reservoir of potential vorticity associated with the stratosphere is as low as 550 hPa. The upper-level instability in culmination with the coastal gyre in the Bay of Mersin, the same initiating structure as Cyclone A, a low-level density current emanating from the Valley of Çakıt and a gap wind moving Eastward originating from the Göksu River Valley aided in the genesis and duration of this vortex.

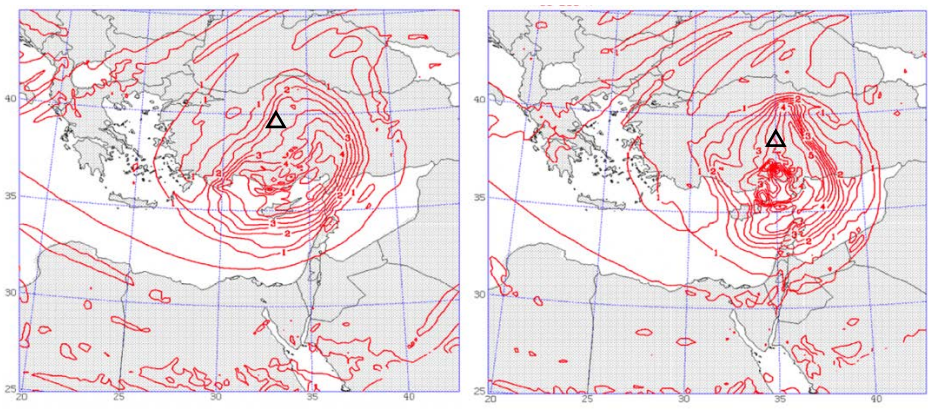

18km WRF potential vorticity at 296 K isentropes (red lines) at 0600 and 1200 UTC 19 February and the location of Cyclone B (black dot), shows region of potential vorticity associated with the upper-level trough overhead.

Figure 21. Upper-level trough on a 296 K potential vorticity surface, Cyclone B

THIS PAGE INTENTIONALLY LEFT BLANK

IV. IDENTIFICATION AND CYCLONE TRACKING

Although synoptic scale cyclogenesis did not occur lee of Middle Taurus Mountains, a host of low-level features to include two sub-synoptic scale cyclones did occur. By plotting the relative area of MSLP and GHT over a time series, it was evident that the low-level signal of these two cyclones diminish over terrain. In Figure 21, Cyclone A has a duration of 10 hours and a max horizontal scale ~30 km, based on the max winds at 925 hPa. Cyclone B has a 11 hours duration and a max horizontal scale of ~50 km when observing both MSLP and GHT.

Figure 22 shows that Cyclone A has a consistent signal of MSLP and GHT until hour 34, at ~500 m in elevation. The MSLP signal diminishes after hour 58 and the GHT signal weakens by hour 60. From the plots of both MSLP and GHT for Cyclone A and B it is evident that elevation and low-level forcing features degrade the signal strength at the surface. The signal of MSLP and GHT are also diluted from the convergent zone and gap wind dynamics that occurs throughout this life cycle.

Examining the anomalous convective regions in the domains with a background of greater than 0 PVU, it is shown in Figure 23 that the cyclone continues even as its signal at the ground ceases. This ability to observe potential vorticity towers and utilize them as tracer for the location and duration of the cyclones can increase the distance that these sub-synoptic systems can be shown to travel. Cyclone A has a consistent signal until hour 35, ~900 m in elevation. Cyclone B has a consistent signal until hour 62, ~800 m in elevation. The dotted line, the height of the potential vorticity tower, in comparison to the area (A), which is the relative magnitude and area of the enclosed region, shows a clear correlation to the magnitude of intensity. Thus, as the potential vorticity vortex stretches so too does relative area increase.

When plotting GHT, MSLP, and the potential vorticity associated with the potential vorticity tower, Figure 24, it is clear that the potential vorticity extends the duration of both Cyclone A and B beyond the MSLP and GHT signature. The duration of Cyclone A is 11

hours, one hour longer than when using both MSLP and GHT. The duration of Cyclone B is 13 hours, 6 hours longer than MSLP and two hours longer than GHT.

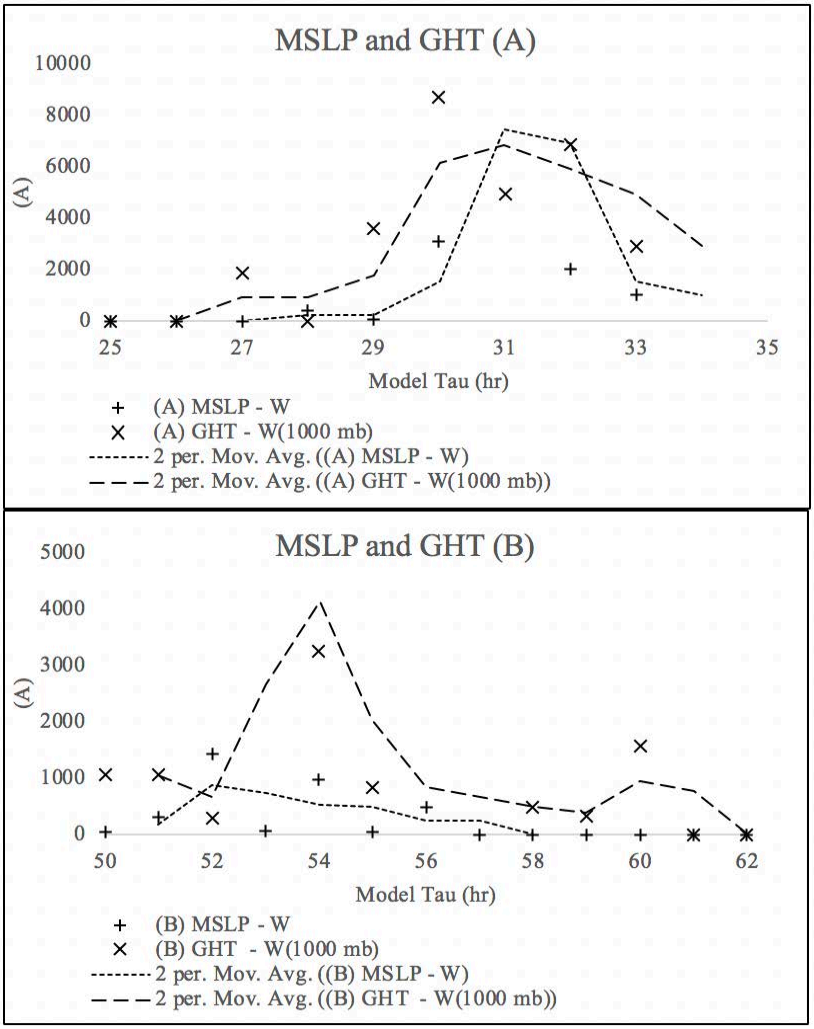

6km WRF analysis, comparing the relative area of the (short dashed line) MSLP (MSLP - W) and GHT (long dashed line) at 1000 hPa (GHT - W(1000 hPa)).

Figure 22. MSLP and GHT (1000 hPa) duration

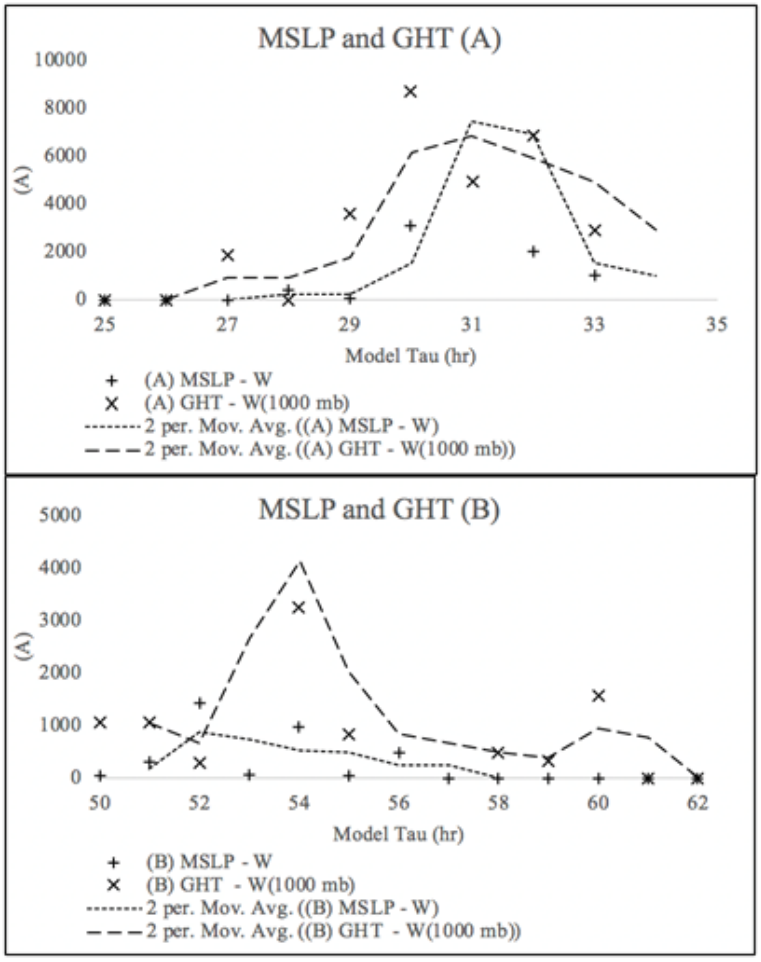

6km WRF analysis, comparing the integrated fields of potential vorticity . The (solid line) is the relative area (PVU-W) and the (dotted line) is the height in km of the vortex (PVU-H).

Figure 23. Potential vorticity tower duration

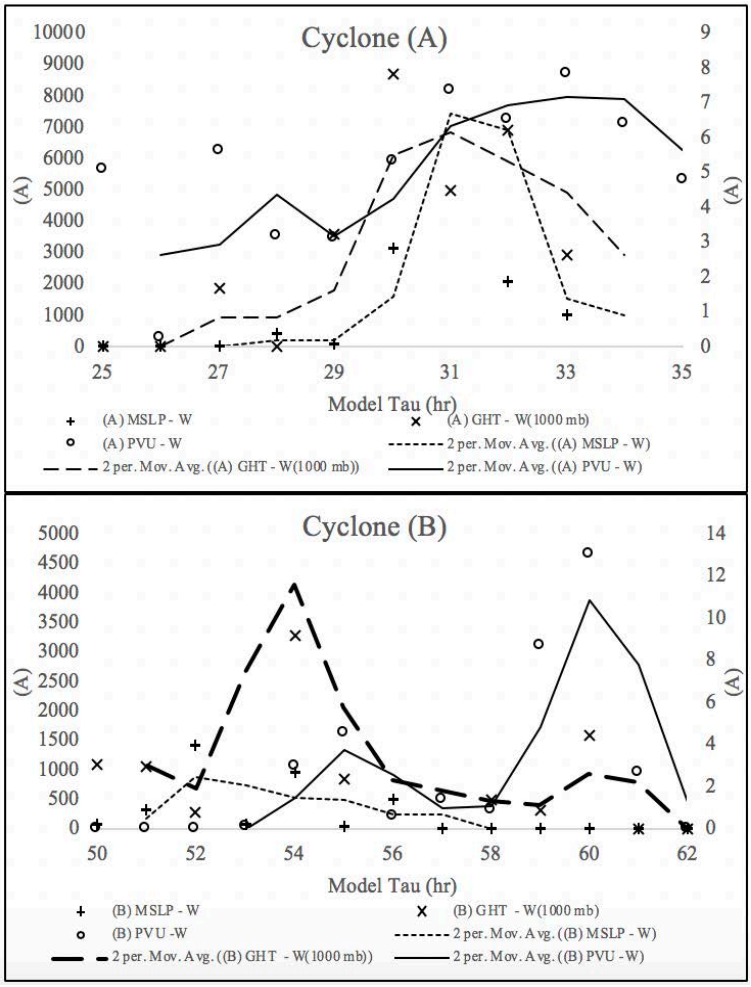

6km WRF analysis, comparing the (solid line) of the relative area of potential vorticity (PVU - W) to the (long dashed line) of GHT at 1000 hPa (GHT - W(1000 hPa)) and (short dashed line) MSLP (MSLP - W)

Figure 24. Comparison of the duration the potential vorticity tower to the to the signal of MSLP and GHT at 1000 hPa

V. CONCLUSION

Through utilizing a fine resolution model, it is evident that synoptic scale lee cyclogenesis, on the order of 200+ km, did not occur lee of the Middle Taurus Mountains. However, sub-synoptic scale lee cyclogenesis on the order of 30-50 km did occur. The topography in this region acts as a convergent zone along the Taurus Mountains with Southerly Flow over the north-easternmost Taurus mountains through the Anatolian Plateau, similarly to the TROWAL (trough of warm air aloft) of a mid-latitude cyclone. For this case study, cyclogenesis "lee of" the Middle Taurus Mountains cyclogenesis occurred two-fold. Cyclone A, in the initial baroclinic environment, and Cyclone B then proceeded to form in the conditionally unstable environment. However, given the average radius of the wind field, these cyclones were only mesoscale in nature.

For this case study, it is shown that the UL-BSL transiting through the Middle Taurus Mountains spawn a myriad of low-level forcing mechanisms and can initiate sub-synoptic cyclogenesis lee of the Middle Taurus Mountains. Comparing two current Mediterranean Sea algorithm thresholds (MSLP and GHT) to the event characterized by the potential vorticity tower, it was shown that instead of using MSLP and GHT to diagnose these small-scale features, potential vorticity towers associated with the cyclones have a higher signal in the tropopause thus extending the detectable life span of the cyclone up to 6 hours. In this highly turbulent boundary layer lee of the Middle Taurus Mountains where many features interact with the GHT and pressure tendencies, using potential vorticity towers as a tracer enables the ability to track sub-synoptic cyclogenetic systems, for a longer period of time.

THIS PAGE INTENTIONALLY LEFT BLANK

LIST OF REFERENCES

Aebischer, U., and C. Schär, 1998: low-level potential vorticity and cyclogenesis to the lee of the Alps. *J. Atmos. Sci.*, **55**, 186–207, doi:10.1175/15200469.

Almazroui, M., and A. Awad, 2016: Synoptic regimes associated with the Eastern Mediterranean wet season cyclone tracks. *Atmos. Res.*, **180**, 92–118.

Alpert, P., and T. Reisin, 1986: An early winter polar air mass penetration to the Eastern Mediterranean. *Mon. Wea. Rev.*, **114**, 1411–1418.

Alpert, P., B. U. Neeman, and Y. Shay-El, 1990: Climatological analysis of Mediterranean cyclones using ECMWF data. *Tellus A*, **42**, 65–77, doi:10.1034/j.1600-0870.1990.00007.x.

Alpert, P., and B. U. Neeman, 1992: Cold small-scale cyclones over the eastern Mediterranean. Tellus A: *Dynamic Meteorology and Oceanography*, **44**:2, 173–179, doi:10.3402/tellusa.v44i2.14952.

Alpert, P., M. Tzidulko, S. Krichak, and U. Stein, 1996: A multi-stage evolution of an ALPEX cyclone. *Tellus*, **48A**, 209–220.

ALPEX (2020). The Alpine experiment. Accessed 25 January 2020, https://www.eol.ucar.edu/field_projects/alpex.

AMS, cited 2019: Lee cyclogenesis. Glossary of Meteorology. [Available online at http://glossary.ametsoc.org/wiki/Lee_cyclogenesis.]

Berg, L. K., W. I. Gustafson, E. I. Kassianov, E. I., and L. Deng, (2013): Evaluation of a modified scheme for shallow convection: Implementation of CuP and case studies. *Mon. Wea. Rev.*, **141**, 134–147, 10.1175/mwr-d-12-00136.1.

Berg, L. K, M. Shrivastava, R. C. Easter, J. D. Fast, E. G. Chapman, and Y. Liu, 2015: A new WRF-Chem treatment for studying regional scale impacts of cloud-aerosol interactions in parameterized cumuli. *Geophys. Model Devel.*, **8**, 409–429. doi:10.5194/gmd-8-409-2015.

Buzzi, A., and A. Speranza, 1983: Cyclogenesis in the lee of the Alps. Lilly K, Gal-Chen T (eds) *Mesoscale Meteorology-Theories, Observations and Models*, NATO ASI series. Reidel, 55–142.

Chen, F., and J. Dudhia, 2001: Coupling an advanced land-surface/ hydrology model with the Penn State/ NCAR MM5 modeling system. Part I: Model description and implementation. *Mon. Wea. Rev.*, **129**, 569–585.

Dudhia, J., 1989: Numerical study of convection observed during the winter monsoon experiment using a mesoscale two-dimensional model, *J. Atmos. Sci.,* **46**, 3077–3107.

Egger, J., 1988: Alpine Lee cyclogenesis: Verification of theories. *J. Atmos. Sci.,* **45,** 2187–2203, doi:10.1175/1520-0469(1988)045<2187:ALCVOT>2.0.CO;2.

Flocas, H., I. Simmonds, J. Kouroutzoglou, K. Keay, M. Hatzaki, V. Bricolas, and D. Asimakopoulos, 2010: On cyclonic tracks over the Eastern Mediterranean. *J. of Climate,* **23,** 5243–5257, doi:10.1175/2010JCLI3426.1.

Hong, S.-Y., J. Dudhia, and S.-H. Chen, 2004: A revised approach to ice microphysical processes for the bulk parameterization of clouds and precipitation, *Mon. Wea. Rev.,* **132**, 103–120.

Hong, S.-Y., and J.-O. J. Lim, 2006: The WRF single-moment 6-class microphysics scheme (WSM6). *J. Korean Meteor. Soc.*, **42**, 129–151.

Hong, S.-Y. and H.-L. Pan, 1996: Nonlocal boundary layer vertical diffusion in a medium-range forecast model. *Mon. Wea. Rev.,* **124**, 2322–2339.

Hong, S.-Y., Y. Noh, and J. Dudhia, 2006: A new vertical diffusion package with an explicit treatment of entrainment processes. *Mon. Wea. Rev.,* **134**, 2318–2341.

Hoskins, B. J., McIntyre, M. E. and Robertson, A. W.1985: On the use and significance of isentropic potential vorticity maps. *Q. J. R. Meteor. Soc.*, **111**, 877–946.

Hoskins, B.J., and K.I. Hodges, 2002, New perspectives on the Northern Hemisphere winter storm tracks. *J. Atmos. Sci.,* **59**(6), 1041–1061.

Jimenez, P., J. Dudhia, J. F. Gonzalez-Ruoco, J. Navarro, J. P. Montavez, and E. Garcia-Bustamente, 2012: A revised scheme for the WRF surface layer formulation. *Mon. Wea. Rev.,* **140**, 898–918.

Jimenez, P. A., and J. Dudhia, 2012: Improving the representation of resolved and unresolved topographic effects on surface wind in the WRF model. *J. Appl. Meteor. Climatol.,* **51**, 300–316.

Kain, J. S., 2004: The Kain-Fritsch convective parameterization: An update. *J. Appl. Meteor.,* **43**, 170–181.

Karaca, M., and S. Dobricic, 1997: Modeling of summertime meso- β scale cyclone in the Antalya Bay. *Geophys. Res. Lett.*, **24**, 151–154, doi:10.1029/96GL03924.

Lacis, A. A., and J. E. Hansen, 1974: A parameterization for the absorption of solar radiation in the earth's atmosphere. *J. Atmos. Sci.,* **31**, 118–133.

Le Treut, H., and E. Kalnay, 1990: Comparison of observed and simulated cyclone frequency distribution as determined by an objective method. *Atmosfera*, **3**, 57–71.

Li, D., E. Bou-Zeid, M. Barlage, F. Chen, and J. A. Smith, 2013: Development and Evaluation of a Mosaic Approach in the WRF-Noah Framework. *J. Geophys. Res.,* **118**, 11918–11935.

Lorente-Plazas, R., P. A. Jimenez, J. Dudhia, and J. P. Montavez, 2016: Evaluating and im- proving the impact of the atmospheric stability and orography on surface winds in the WRF model. *Mon. Wea. Rev.*, **144**, 2685–2693.

Mlawer, E. J., S. J. Taubman, P. D. Brown, M. J. Iacono, and S. A. Clough, 1997: Radiative transfer for inhomogeneous atmosphere: RRTM, a validated correlated-k model for the long- wave. *J. Geophys. Res.,* **102 (D14)**, 16663–16682.

NCEI (2020). Climate Forecast System. Accessed 25 January 2020, https://www.ncdc.noaa.gov/data-access/model-data/model-datasets/climate-forecast-system-version2-cfsv2.

Noh, Y., W.G. Cheon, S.-Y. Hong, and S. Raasch, 2003: Improvement of the K-profile model for the planetary boundary layer based on large eddy simulation data. *Bound.-Layer Meteor.,* **107**, 401–427.

Nuss, W., and S. Drake, 1990: *VISUAL Meteorological Diagnostic and Display Program*, Naval Postgraduate School Department of Meteorology, 51 pp.

Palmen, E., and C.W. Newton, 1969: *Atmospheric Circulation Systems: Their Structure and Physical Interpretation.* Academic Press, 603 pp.

Petterssen, S., and S. J. Smebye, 1971: On the development of extratropical cyclones. Q. *J. R. Meteor. Soc.*, **97**, 457482, doi:10.1002/qj.49709741407.

Skamarock, W. C., Klemp, J. B., Dudhia, J., Gill, D. O., Liu, Z., Berner, J., … Huang, X. -yu. (2019). *A Description of the Advanced Research WRF Model Version 4* (No. NCAR/TN-556+STR). doi:10.5065/1dfh-6p97.

Stephens, G. L., 1978: Radiation profiles in extended water clouds. Part II: Parameterization schemes, *J. Atmos. Sci.,* **35**, 2123–2132.

Tafferner, A., 1990: Lee cyclogenesis resulting from the combined outbreak of cold air and potential vorticity against the Alps. *Meteor. Atmos. Phys.,* **43,** 31–47.

Tafferner, A., and J. Egger, 1990: Test theories of lee cyclogenesis: ALPEX cases. *J. Atmos. Sci.,* **47:**22, 2417–2428.

Trigo, I. F., G. R. Bigg, and T. D. Davies, 2002: Climatology of Cyclogenesis Mechanisms in the Mediterranean. *Mon. Wea. Rev.*, **130**, 549–569, doi:10.1175/15200493.

Trigo, I. F., 2006: Climatology and Interannual Variability of Storm-Tracks in the Euro-Atlantic sector: A comparison between ERA-40 and NCEP/NCAR Reanalyses. *Climate Dynamics*, **26**, 127–143, doi:10.1007/s00382-005-0065-9.

Wilson, T. H., and R. G. Fovell, 2018: Modeling the evolution and life cycle of radiative cold pools and fog. *Wea. and Forecasting*, **33**, 203–220.

WRF (2020). Weather research and forecasting model. Accessed 10 Jan 2020, https://www.mmm.ucar.edu/weather-research-and-forecasting-model.

INITIAL DISTRIBUTION LIST

1. Defense Technical Information Center
   Ft. Belvoir, Virginia

2. Dudley Knox Library
   Naval Postgraduate School
   Monterey, California